MODELLING AND CONTROL OF HYPERSONIC AIRCRAFT VEHICLES

A Thesis Submitted to
the Graduate School of Engineering and Sciences of
İzmir Institute of Technology
in Partial Fulfillment of the Requirements for the Degree of

MASTER OF SCIENCE

in Electronics and Communication Engineering

by
Barış BIDIKLI

December 2012
İZMİR

We approve the thesis of **Barış BIDIKLI**

Examining Committee Members:

Prof. Dr. F. Acar SAVACI
Department of Electrical and Electronics Engineering
İzmir Institute of Technology

Assoc. Prof. Dr. Serdar İPLİKÇİ
Department of Electrical and Electronics Engineering
Pamukkale University

Assoc. Prof. Dr. Enver TATLICIOĞLU
Department of Electrical and Electronics Engineering
İzmir Institute of Technology

14 December 2012

Assoc. Prof. Dr. Enver TATLICIOĞLU
Supervisor
Department of Electrical and Electronics Engineering
İzmir Institute of Technology

Prof. Dr. F. Acar SAVACI
Head of the Department of
Electrical and Electronics Engineering

Prof. Dr. R. Tuğrul SENGER
Dean of the Graduate School of
Engineering and Sciences

To woman of my life, my mom.

ACKNOWLEDGMENTS

I would like to thank my mom Özlem S. KIRAL and my grandma A. Feral KIRAL for their endless support and encouragement throughout my life.

I would like to thank my friends who are closer than brothers or sisters to me; İlter AKDER, B. Orkan OLCAY, K. Merve DOĞAN, M. Doğan ELBİ and Ferhan KULOĞLU ELBİ.

I would like to thank Gizem AKÇAY for her support and help. I believe she deserves a special place.

I would like to thank Bahar CİVAN for her understanding, confidence and support. I believe she is one of the most important people throughout this process.

I would like to express my gratitude to Assoc. Prof. Dr. Serdar İPLİKÇİ for his guidance, leadership and support.

I would like to thank the thesis supervisor Assoc. Prof. Dr. Enver TATLICIOĞLU for his guidance, support and trust throughout this thesis.

Finally, I would like to thank TÜBİTAK BİDEB for providing financial support for my works as a sponsor.

ABSTRACT

MODELLING AND CONTROL OF HYPERSONIC AIRCRAFT VEHICLES

The increasing number of works on hypersonics and the recent interest of Ministry of Defense on developing a hypersonic missile are amongst the main motivations behind this thesis. Research on hypersonics seems to divide into two main categories: deriving dynamic models for HSVs and designing model-based controllers.

Initially, we decided to investigate the control problems associated with HSVs. However, due to the restrictions imposed by the leading sponsors of hypersonic research (such as NASA, US AF, US DoD, DARPA, etc), researchers did neither publish nor share the model parameters for HSVs. As a result, our initial focus was deriving a dynamic model for an HSV.

Firstly, modelling approaches for HSVs and we noticed that it is extremely hard to directly obtain the HSV dynamic model parameters. In addition to this, the HSV nonlinear dynamic model which was commonly mentioned in the literature is not related to the control inputs directly. As a result, the linearized HSV dynamic models were investigated, and the linear parameter varying model was derived.

Next, control problems associated with the HSVs are investigated. Due to the highly complicated and time-varying nature of their dynamics, designing a robust control law is aimed. The main reason behind choosing to design a robust control law was that the robust controllers usually require minimum knowledge about the HSV dynamics. The stability of the proposed robust control law is then investigated via Lyapunov-based techniques and the tracking error is driven to the origin exponentially fast by using designed controller.

ÖZET

HİPERSONİK HAVA ARAÇLARININ MODELLENMESİ VE KONTROLÜ

Hipersonikler ile ilgili yapılan çalışmaların artması ve Milli Savunma Bakanlığı'nın hipersonik füze geliştirmek amacı ile son dönemde başlattığı çalışmalar, bu tezin arkasındaki ana motivasyonlar olarak sayılabilir. Hipersoniklerle ilgili araştırmalar incelendiğinde iki ana kısıma ayrıldığı görülmektedir. Bunlar; dinamik model eldesi ve model temelli denetim çalışmalarıdır.

Bu konuyla ilgili başlangıç hedefimiz HSV'ler ile ilgili denetim problemlerini araştırmaktı. Bununla birlikte, hipersonik araştırmalarının ana sponsorlarının (NASA, US AF, US DoD, DARPA, vb.) kısıtlamalarından ötürü araştırmacıların model parametrelerini yayınlayamamaları ve paylaşamamaları, başlangıç hedefimizi HSV dinamik modelinin elde edilmesi haline getirmiştir.

İlk olarak HSV ile ilgili modelleme yaklaşımları incelenmiş ve HSV dinamik model parametrelerinin doğrudan bulunmasının oldukça zor olduğu tespit edilmiştir. Buna ek olarak, literatürde yaygın olarak kullanılan HSV dinamik modeli, denetim girişleri ile doğrudan ilişkilendirilmemektedir. Sonuç itibariyle doğrusallaştırılmış HSV dinamik modelleri araştırılmış ve doğrusal parametre değişimli model elde edilmiştir.

Bir sonraki adım olarak HSV ile ilgili denetim problemleri araştırılmıştır. HSV dinamiklerinin yüksek miktarda karışık ve zamana bağlı doğasından ötürü, gürbüz bir denetleyici tasarımı hedeflenmiştir. Gürbüz denetleyicinin seçilmesinin arkasındaki ana etmen, bu tip denetleyicilerin HSV dinamikleri hakkında minimum bilgiye ihtiyaç duymasıdır. Önerilen gürbüz denetleyicinin kararlılığı Lyapunov temelli yöntemler yardımıyla ortaya ve bu tasarlanan denetleyici kullanılarak hata değerlerinin üstel bir hızla orjine gitmesi sağlanmıştır.

TABLE OF CONTENTS

LIST OF FIGURES

Figure **Page**

LIST OF SYMBOLS

M ..... Mach Number
a ..... Speed of Sound
v ..... Velocity of the Source
$\bar{q}$ ..... Dynamic Pressure
L_T ..... Total Length of HSV
L_1 ..... Forebody Length of HSV
L_2 ..... Aftbody Length of HSV
h_i ..... Engine Inlet Height of HSV
τ_{1U} ..... Upper Forebody Angle of HSV
τ_{1L} ..... Lower Forebody Angle of HSV
τ_2 ..... Tail Angle of HSV
I_{yy} ..... Moment of Inertia
ω_{1n} ..... First Flexible Mode of HSV
ω_{2n} ..... Second Flexible Mode of HSV
ω_{1n} ..... Third Flexible Mode of HSV
ξ ..... Flexible Mode Damping of HSV
L ..... Lift
T ..... Thrust
D ..... Drag
M ..... Pitching Moment
N_i ..... Generalized Forces
m ..... HSV Total Mass
g_0 ..... Acceleration due to Gravity at Sea Level
R_E ..... Radius of the Earth
v ..... Velocity
γ ..... FPA
h ..... Altitude
q ..... Pitch Rate
θ ..... Pitch Angle
η_i ..... Flexible Body States
$\dot{\eta}_i$ ..... Flexible Body Velocities
δ_e ..... Rearward Situated Elevator

δ_e . . . . . Forward Situated Canard

$\phi_i(x)$ . . . . . i^{th} Mode Shape

V_e . . . . . Speed of Flow Exiting the Engine

V_∞ . . . . . Freestream Speed

p_e . . . . . Pressure at the Exit of the Internal Nozzle

p_∞ . . . . . Freestream Pressure

$\dot{m}_a$ . . . . . Mass Airflow into the Engine

A_e . . . . . Engine Exit Area Per Unit Span

F_x . . . . . Sum of Forces in the x Direction

F_z . . . . . Sum of Forces in the z Direction

F_j . . . . . j^{th} point Load Acting at Point x_j on the Vehicle

$Lift_{viscous}$ . . . . . Lift Due to Viscous Effects

$Drag_{viscous}$ . . . . . Drag Due to Viscous Effects

$F_{x,l}$ . . . . . Lower Forebody Force, x Direction

$F_{z,l}$ . . . . . Lower Forebody Force, z Direction

$F_{x,u}$ . . . . . Upper Forebody Force, x Direction

$F_{z,u}$ . . . . . Upper Forebody Force, z Direction

$F_{x,inlet}$ . . . . . Engine Inlet Force, x Direction

$F_{z,inlet}$ . . . . . Engine Inlet Force, z Direction

$F_{x,e}$ . . . . . Exhaust Force of Aftbody, x Direction

$F_{z,e}$ . . . . . Exhaust Force of Aftbody, z Direction

$F_{x,cs}$ . . . . . Elevator Force, x Direction

$F_{z,cs}$ . . . . . Elevator Force, z Direction

$F_{x,unsteady}$ . . . . . Unsteady Force, x Direction

$F_{z,unsteady}$ . . . . . Unsteady Force, z Direction

$F_{z,b}$ . . . . . Pressure on Bottom of Vehicle, z Direction

$M_{unsteady}$ . . . . . Moment Due to Unsteady Pressure Distribution

$M_{viscous}$ . . . . . Moment Due to Viscous Effects

M_f . . . . . Moment Due to Lower Forebody Forces

M_u . . . . . Moment Due to Upper Forebody Forces

M_{inlet} . . . . . Moment Due to Turning Force at Engine Inlet

M_{cs} . . . . . Moment Due to Control Surface Forces

M_b . . . . . Moment Due to Engine Base Force

$\overline{c}$ . . . . . Mean Aerodynamic Chord

S . . . . . Reference Area

z_T . . . . . Thrust–to–Moment Coupling Coefficient

A_m,B_m . . . . . Constant State and Input Matrices for Reference Model

$\delta(\cdot)$ . . . . . Reference Input

$y_m(\cdot)$ . . . . . Reference Output

$e(\cdot)$ . . . . . Output Tracking Error

$r(\cdot)$ . . . . . Filtered Output Tracking Error

γ . . . . . Diagonal, Positive Definite Constant Gain Matrix

$z(\cdot)$ . . . . . Combined Error Signal

$\|\cdot\|$ . . . . . Standard Euclidean Norm

$S(\rho(t))$ . . . . . Positive Definite Symmetric Matrix

D_D . . . . . Diagonal Matrix with Entries Being ± 1

$U(\rho(t))$ . . . . . Unity Upper Triangular Matrix

$\underline{\mathrm{m}}$,$\overline{m}$ . . . . . Positive Bounding Constants

$N(x,t)$ . . . . . An Auxiliary Signal

$\overline{N}(\cdot)$,$\widetilde{N}(e,\dot{e},r,t)$ . . . . . Auxiliary Signals Obtained from N

β . . . . . Constant Positive Definite Diagonal Gain Matrix

$\mathrm{Sgn}(\cdot)$ . . . . . Vector Signum Function

k_q,$k_{d,i}$ . . . . . Constant Positive Control Gains

$\rho_{\widetilde{N}}$ . . . . . Positive Constant

$\zeta_{\overline{N}_i}$,ζ_{Θ_i} . . . . . Positive Bounding Constants

$V_1(z)$ . . . . . Lyapunov Function

ϵ . . . . . Positive Constant

LIST OF ABBREVIATIONS

NASA . . . . . National Aeronautics and Space Administration
TSTO . . . . . Two–Stage–to–Orbit
HSV . . . . . Hypersonic Vehicle
NASP . . . . . National AeroSpace Plane
SSTO . . . . . Single–Stage–to–Orbit
US DOD . . . . . United States Department of Defense
AFRL . . . . . Air Force Research Laboratory
ADSTO . . . . . Australian Defence Science and Technology Organization
HTV . . . . . Hypersonic Technology Vehicle
USAF . . . . . United States Air Force
DARPA . . . . . Defense Advanced Research Projects Agency
HCV . . . . . Hypersonic Cruise Vehicle
CFD . . . . . Computational Fluid Dynamics
LPV . . . . . Linear Parameter Varying
AoA . . . . . Angle–of–Attack
FPA . . . . . Flight Path Angle
SSA . . . . . Side–Slip–Angle
FER . . . . . Stoichiometrically Normalized Fuel Equivalence Ratio
FTA . . . . . Flight Total Angle
LCO . . . . . Limit Cycle Oscillations

CHAPTER 1

INTRODUCTION

Humans try to find efficient ways to move faster and higher. On the other hand, commercial groups want a more reliable way of putting payload in the low earth orbit. While defense organizations want high speed and high altitude weaponry. And all of these seem more reachable with hypersonic aircraft vehicles. The main question is "What is Hypersonic?". To answer this question, we first explain the different flight regimes that includes hypersonic.

1.1. Speed Regimes of the Flight

After the invention of the airplane, designers and engineers created new ones for a wide variety of applications. Airplanes become a part of the daily life and are used regularly to ship cargo and to transport people. As a result of the developments in the aircraft industry, the speed of aircrafts has increased and one way to classify aircrafts is based on the speed regimes of the flight. There are five basic reachable speed regimes and two additional unreachable speed regimes which are categorized with respect to the velocity to speed of sound ratio. In order to clearly understand the difference between these speed regimes, we will first explain the Mach number.

1.1.1. Mach Number

In fluid mechanics, Mach number is a dimensionless number which is invented by Austrian physicist and philosopher Ernst Mach and denotes the velocity to speed of sound ratio. The equation of the Mach number is given as

$$M \triangleq \frac{v}{a} \tag{1.1}$$

where $v \in \mathbb{R}$ denotes the velocity of the source, $a \in \mathbb{R}$ denotes the speed of sound and $M \in \mathbb{R}$ denotes the Mach number. Speed regimes of the flight are classified in terms of the Mach number as shown in Table 1.1. The additional unreachable speed regimes that are shown in the last two rows of the table (High–Hypersonic and Re–entry

Speeds) are defined by the National Aeronautics and Space Administration (NASA) and all information about them can be considered as theoretical. According to the information provided by the NASA, it can be easily said that hypersonic is not only the last basic speed regime but also the highest speed regime that was reached.

Table 1.1. Classification of Mach Regimes

Regime	Mach	mph	m/s	ft/s
Subsonic	<0.8	<610	<270	<810
Transonic	0.8–1.2	610–915	270–410	810–1225
Supersonic	1.2–5.0	915–3840	410–1710	1225–5150
Hypersonic	5.0–10.0	3840–7680	1710–3415	5150–10250
High–Hypersonic	10.0–25.0	7680–16250	3415–8465	10250–25400
Re–entry Speeds	>25.0	>16250	>8465	>25400

Now, we try will provide some extra information about five basic speed regimes.

1.1.2. Subsonic

The early development of human flight which included air vehicles such as kites, balloons, and gliders were in this speed range. These unpowered aircrafts were very slow. After the development of relatively lightweight engines, the speed of these early airships and winged aircrafts increased, but the available materials, knowledge and technology limited these aircrafts to operate at low speeds.

Specifically, the limitations of the available engines enforced these vehicles to be light weight. To build light weight structures, designers used external bracing. That, and the open fuselage designs of the day, resulted in vehicles with high drag. As a result, even at low speeds such as 50 mph, the produced drag overcame the available thrust.

As in the early days, since the general light weight structure, these aircrafts were limited by the power available from the small, light engines. These aircrafts were generally faster than their predecessors because of stronger, light weight materials (nylon and aluminum), improved knowledge of aircraft design, and improved engines (with a higher ratio of power–to–weight).

1.1.3. Transonic

In order to build faster aircrafts, several areas or technologies had to be improved. First, the drag had to be reduced substantially. This was accomplished largely by developing enclosed, streamlined fuselages and stronger wings that did not require external bracing. These resulted the structures to be stronger, but not heavier at the same time. Thus, materials and structures were developed with a higher strength to weight ratio. Next, the thrust had to be greatly increased without increasing the weights of the engines, and thus, resulting in engines with a higher power–to–weight ratio. All of these areas improved steadily. For instance, a new engine might be developed with 50 percent more power that weighted only 25 percent more (which obviously has a higher power–to–weight ratio) however since it weighted more, the fuselage would have to be stronger and heavier to carry this extra weight. As a result, the aircraft might *not* really be faster until it could be designed to be lighter. On the other hand, through the use of new tools such as wind tunnels and a lot of basic research, the knowledge of aerodynamics improved.

The vehicles that are found in this regime are limited by the source of the thrust and, to a lesser extent, the drag. The engines are almost all propeller types, and the wings are almost all straight and fairly thick. Propeller crafts like Fokker, Junkers, Cessna and Beechcraft can be given examples of the vehicles in this category.

1.1.4. Supersonic

With the desire to fly faster and primarily for military applications, aeronautics technologies were developed to fly above Mach 1. However these aircrafts were still very expensive to operate and most were for military use only. To date, only one aircraft, namely the Concorde, achieved commercial transportation above Mach 1.

Efforts are still underway to develop new technologies so that a more cost–effective supersonic airplane can be built in the future. Supersonic aircrafts have special high performance jet engines that can provide a good amount of thrust, have highly–sweeper very thin wings, and utilize novel materials to provide strength.

Early fuselages have thin bodies. The thinning of the fuselages helps reduce the drag when flying near the speed of sound. Because of the reducing drag, it is relatively easier to fly above Mach 1 than near Mach 1. Heavy engines are needed to provide the necessary thrust to push the airplane through the air at such high speeds. The wings

are super thin and swept to slice through the air while making as little disturbance as possible. The most modern supersonic aircraft spend so little time near Mach 1 and have such powerful engines, that they are not shaped as much like old thin bodies. Still, these aircraft have sleek overall shapes that are carefully designed to minimize supersonic drag.

It is interesting that airplanes designed to fly supersonically do not perform very well at subsonic speeds. The specific features that let them fly fast do not work well when they fly slowly. In fact, flight at the lowest speeds, such as during takeoff or landing, is an extra challenge when designing these aircrafts. Although they were not used for global transportation F–15 Eagle and the SR–71 can be given as examples for this category. The other example, above mentioned Concorde, was used for global transportation successfully. It is noted that according the some references, its flight was recorded as a supersonic flight (Mach 1.3) while some references recorded it as a transonic flight (Mach 1.1).

1.1.5. Hypersonic

With the advance of the rocketry, the first hypersonic vehicles were developed. Rockets can travel at these speeds when they accelerate into the Earth's orbit. Also, the reentry capsules (such as those in the Apollo program) travel at these speeds as they descend from orbit.

The best known examples of hypersonic flight vehicles are the rocket-powered X–15, NASA's X–43A prototype and the space shuttle which can travel at all speed regimes when it reenters the Earth's atmosphere. In addition to these examples, there are lots of theoretical and experimental works. Research programs (especially the ones in the USA) are underway to develop new engines that can operate at these speeds, so new aircrafts can be designed to cruise in this speed regime.

National AeroSpace Plane (NASP)'s programs resulted in three experimental aircrafts, the X–30, the X–33 and the X–34, and another project, namely as Falcon, resulted in three experimental vehicles, the HTV–1, the HTV–2 and the HTV–3. It is noted that, there are no commercial or military aircrafts today that can cruise at these speeds. A few prototypes can be flight only up to now and most of them couldn't reach hypersonic speeds efficiently, couldn't do their second flight due to damages at the first flight or couldn't finish their first flight successfully due to communication losses or lack of control. We would like to highlight that, it is a tremendous challenge to design an airplane shape and an engine that can take off subsonically, accelerate through supersonic speeds, and cruise efficiently hypersonically in an efficient manner.

What's faster than hypersonic? Hypersonic flight occurs at very high altitudes where the air is extremely thin which helps to reduce the drag and the heating due to friction. The need for thin air at high altitudes and high speeds are major reasons that make it so difficult to design engines for these aircrafts. To fly faster than hypersonic speed requires even thinner air at higher altitudes, and at these altitudes, a vehicle is essentially outside the atmosphere and should more correctly be called a spacecraft. Thus, the space shuttle is both a spacecraft and an aircraft.

1.2. Motivations on Conducting Research on HSVs

With the historic 2004 SCRAMjet–powered Mach 7 and Mach 10 flights of the NASA X–43A experimental vehicle, hypersonic research has seen a resurgence. This is most probably attributable to the fact that air–breathing hypersonic propulsion is viewed as the next critical step towards achieving reliable and affordable access to space, and for global transportation. Both of these objectives have commercial as well as military applications.

Air–breathing HSVs are seen as a feasible solution to provide safe and affordable space travel. Hypersonic flight is being aggressively pursued as a capability to traverse the world in a few hours. The class of vehicles under consideration utilize a design in which a wedge–shaped fuselage provides lift and acts as an inlet for the SCRAMjet engine. This configuration and its associated aeropropulsive characteristics were successfully demonstrated on the X–43 prototype.

From a design perspective, while rocket–based (combined cycle) propulsion systems are needed to reach orbital speeds, these systems are much more expensive to operate since they must carry oxygen (which is expensive particularly when traveling at lower altitudes through the troposphere). Current rocket–based systems also do not exhibit the desired levels of reliability and flexibility (e.g. they don't have airplane–like takeoff and landing options). For these reasons, much emphasis have been placed on the two–stage–to–orbit (TSTO) designs that have two different stage to provide propulsion consecutively. In this design, first stage is responsible for accelerating the vehicle and the second stage is responsible for continuing to orbit under its own power. HSVs utilize a turbo–ram–SCRAMjet combined cycle in the first stage and a rocket–SCRAMjet in the second stage.

While the designs of HSVs are maturing due to aeropropulsive interactions between the fuselage and the engine; there are still associated challenges that need to be

researched significantly. For example, aerothermoelastic characteristics must further be addressed. Since any displacement of the fuselage significantly affects the performance of the engine, vibration attenuation is an another critical requirement for these vehicles.

Due to the highly complicated and time–varying nature of their dynamics, which is mostly because of the significant effects of the temperature changes on the structural dynamics, control of HSVs is a challenging research area. A commonly utilized control approach which is named as multi–loop control architecture is formulated to contain compensators for vibration suppression, maneuvering and engine control. This control architecture directly matches a model of the open–loop HSV dynamics which couples aerodynamics and structural dynamics with engine dynamics. The multi–loop control architecture consists of three controllers: an inner–loop controller, an outer–loop controller and an engine controller. The inner–loop controller is used to actively augment damping of the structural modes criteria, and the outer–loop controller is then used to achieve rigid–body performance. Finally, an engine controller operates continuously to guarantee proper propulsion despite variations in the flight dynamics. The multi–loop control architecture includes gain–scheduled elements and adaptive elements. The gain–scheduled elements represent pre–flight designs based on high fidelity models, whereas the adaptive elements are used to cancel any residual errors. Essentially, the adaptive elements only affect the system when aerothermoelastic dynamics vary beyond theoretical ranges and when the gain–scheduled controller is unable to achieve the desired performance of either the flight path or engine propulsion.

1.3. Literature Survey

In this section, the past research in the literature on HSVs is categorized as: experimental research that contains the significant practical works about HSVs, in an historical order, and theoretical research that contains the significant modelling and control works about HSVs which can be found during the literature search.

1.3.1. Experimental Research on Hypersonic

Although, the most important work was performed by NASA with X–43A prototype, we can encounter various important HSV works before and after that. These works that include X–43A can be summarized as follows.

1.3.1.1. General Research on SCRAMjet Propulsion

NASA's works about this topic have started in the middle of 1960's and have continued for over 50 years Fidan et al. (2003); Voland et al. (2005). In 1960's, NASA built and tested a hydrogen–fueled and cooled SCRAMjet engine that verified SCRAMjet efficiency, structural integrity, and first generation design tools. Then, in 1970's a fixed–geometry, airframe–integrated SCRAMjet flowpath (capable of propelling a HSV from Mach 4 to Mach 7) was designed and demonstrated in wind tunnel tests. After this point, SCRAMjet engine technology was used to develop waverider which provided the basis for HSV developments.

1.3.1.2. NASP X–30

This single–stage–to–orbit (SSTO), hydrogen fueled waverider was developed by United States Department of Defence (US DOD) and NASA between the years 1984–1996. Despite the fact that no flights took place, a significant amount of research was accomplished on aerothermoelastic propulsion R.McClinton (2007); Anderson (2002); Fidan et al. (2003); Heeg et al. (1993); Gilbert et al. (1990); Heeg et al. (1993); Potozky et al. (1988). These aerothermoelastic propulsion effects were researched by a group of 500 engineers and scientists who were involved in this project Fidan et al. (2003); Kumar et al. (2001).

1.3.1.3. Single–Stage–to–Orbit Technology Demonstrators

The X–33 and X–34 would follow NASP X–30. The X–33 was developed during a project named Skunk by American global aerospace, defense, security, and advanced technology company Lockheed Martin and was initially planned as an unmanned vehicle. This triangularly shaped lifting body rocket–engine powered technology demonstrator was able to reach 15 times the speed of sound and 250 kft altitude. The much smaller prototype X–34 was planned as an unmanned vehicle too. This rocket–engine powered technology demonstrator intended to operate like the space shuttle and was able to reach 8 times the speed of sound and 250 kft altitude.

1.3.1.4. HyShot Flight Program

Supersonic combustion of a SCRAMjet in flight was demonstrated at July 30, 2002 (HyShot II) and March 25, 2006 (HyShot III) by the University of Queensland Center for Hypersonics Smart et al. (2006). During each flight, a two–stage, hydrogen fueled Terrier–Orion Mk70 rocket was used to boost the payload to 330 km altitude. Engine measurements demonstrated that at altitudes between 23 km and 35 km when the payload carrying re–entry Orion reached 7.6 times the speed of sound. Flight results were correlated with the University of Queenslands T4 shock tunnel. Thus far, the center has been involved with five flights – the last being on June 15, 2007 (HyCAUSE) Walker et al. (2008).

1.3.1.5. NASA's Hyper–X Flight Program

NASA's Hyper–X Flight program can be seen as the most important development program for the hypersonic technology. This program was resulted with two important products. The X–43A which is seen as the best HSV prototype ever were developed during this program and two different SCRAMjet–powered hypersonic flights at Mach 7 and Mach 10 (actually Mach 6.83 and Mach 9.8) were realized by using it. They are seen as the most important hypersonic flights still Peebles (2008); R.McClinton (2007); Rausch et al. (1997). Also, the other important product of this program namely as SR–71 Blackbird was reached Mach 5 while the maximum reachable turbojet speed was recorded as Mach 3.2.

1.3.1.6. HiFIRE: The Hypersonic International Flight Research Experimentation

This program is an ongoing collaboration between NASA, Air Force Research Laboratory (AFRL), Australian Defence Science and Technology Organization (ADSTO), Boeing Phantom Works, and the University of Queensland Dolvin (2008). It will involve 10 flights over 5 years. HiFIRE flights will focus on the goal of understanding the fundamentals of hypersonic phenomena.

1.3.1.7. X–51A SCRAMjet Demonstrator Waverider

The Boeing X–51A is being developed as an expendable hydrocarbon fueled SCRAMjet engine demonstrator waverider vehicle by AFRL, Boeing, and Pratt and Whitney Hank et al. (2008). It reached Mach 7 in the tests in 2009.

1.3.1.8. Falcon

The main purpose of this project is to develop a series of incremental hypersonic technology vehicle (HTV) demonstrators and it has continued with United States Air Force (USAF) and Defense Advanced Research Projects Agency (DARPA) cooperation since 2003. Within the scope of this project HTV–1, HTV–2, HTV–3X demonstrations were designed to develop technologies for a future reusable hypersonic cruise vehicle (HCV) specifically designed for prompt global reach missions.

1.3.2. Overview of Theoretical Research on Hypersonics

There have been several papers in the literature that have discussed challenges associated with the dynamics of hypersonic vehicles. A detailed analytical model of the longitudinal dynamics was undertaken by Chavez and Schmidt (1994). A slightly different approach to develop a model was undertaken by Bolender and Doman (2005, 2007a, 2006) which was further developed by Williams et al. (2006a); Culler et al. (2007). A computational fluid dynamics (CFD) approach was also utilized to develop a model of the hypersonic vehicle Bolender and Doman (2006).

In the past few years, a considerable effort has been made by the USAF and NASA to improve development and design of HSVs.Notwithstanding the recent success of NASA's X–43A experimental vehicle, the design of robust guidance and control systems for hypersonic vehicles is still an open problem mostly due to the peculiarity of the vehicle dynamics. In addition to the interactions between flexible and rigid body modes, the dynamics of air–breathing hypersonic vehicles include couplings between the engine and the flight dynamics. On the other hand, the slender geometries and light structural weights required for these aircrafts cause significant flexible effects, and a strong coupling between propulsive and aerodynamic forces that result from the integration of the SCRAMjet engine. In addition, due to the dependence of the vehicle characteristics to the

flight conditions (such as thermal effects on the structure), significant uncertainties affect the vehicle model.

For the control design, there are several issues that must be addressed. The controller must account for strongly coupled aerodynamics–propulsion dynamics and actively suppress modal vibrations. Also, the aerothermoelastic effects cannot be ignored in a hypersonic flight and must be compensated.

Using the modelling approaches in the literature as a fixed design, several control approaches have been considered including H_∞ control Buschek and Calise (1994), μ synthesis Buschek and Calise (1993) control, and linear parameter varying (LPV) control Lind (2001); Wilcox et al. (2010a); Bhat (2008); Wilcox (2010). Various other control strategies such as adaptive control Fiorentini et al. (2007); Sigthorsson et al. (2008); Kuipers et al. (2007a); Sigthorsson et al. (2006) and other linear control techniques Huo et al. (2006); Groves et al. (2005, 2006), have also been discussed in the literature.

Several past studies focused on design of guidance and control systems based on linearized dynamical models. These studies considered control solutions of various complexity. Implicit model–following control methods have been considered in Sigthorsson et al. (2006); Groves et al. (2005, 2006) for the linearized versions of the dynamic model in Bolender and Doman (2007a), and adaptive control techniques have been considered in Kuipers *et al*. Kuipers et al. (2007b) for the CFD–based model in Mirmirani et al. (2005).

A thorough survey of difficulties encountered in modelling and control of HSVs. For example, with a focus on aerothermoelasticity, a Lyapunov–based exponential tracking control performance with aerothermoelastic effects by using LPV form was presented in Wilcox et al. (2010a); Wilcox (2010). Different ways of nonlinear adaptive controller design by compensating aerothermoelasticity were presented in Fiorentini et al. (2007); Bolender et al. (2007); Bhat (2008).

1.3.3. Modelling and Control Challenges

It is clear that modelling is the most important step for an efficient controller design. Although, there are good developments available in the literature, modelling and control is still an open problem because of the some challenges. In this subsection, we try to provide some information about modelling and control challenges which were encountered in past HSV researches.

1.3.3.1. Lifting Body and Waverider Dynamics

Integrated–airframe air–breathing propulsion lifting body designs Heiser et al. (1994b) and their special subclass namely as waverider designs Anderson (2006) are widely used in HSVs and attracting too much attention in the literature. Although, they are the most appropriate structure for the hypersonic flights, they can't be modelled properly because of their specific geometric structures. Because of the mentioned reasons, they can be expressed approximately in the dynamic model.

1.3.3.2. The Main Purpose of the Selection of Waveriders

Generally, lift–to–drag ratio decreases with increasing Mach and is particularly low for hypersonic vehicles Anderson (2006). An independent shock wave affects the conventional HSVs along the leading edge and as a result of this, they have a reduced maximum lift–to–drag ratio. This situation is particularly very effective in blunt lifting body designs.

In contrast, HSVs that have waverider designs have an attached shock wave along the leading edge and appear to ride the bow shock wave Anderson (2006). As a result of this, waveriders can exhibit higher lift–to–drag ratio for a given angle–of–attack (AoA), and can be flown at lower values of AoA too. On the other hand, a higher maximum lift–to–drag ratio is desirable to maximize the range Anderson (2006). Therefore, waveriders are required for global reach cruise applications.

1.3.4. Aero–Thermo

Slender body type can reduce drag while increasing structural heating (e.g. nose heating) and is inversely proportional to the nose radius. Since heat–driven structure is preferred for drag–driven structures, most hypersonic vehicles possess blunt noses. This is because within the hypersonic regime, heating varies cubicly with speed, while drag varies quadratically Anderson (2006).

1.3.4.1. SCRAMjet Propulsion

In contrast to regular jets which have a compressor, SCRAMjets (which rely on forebody compression) have no moving parts. As a result of this, they can operate over a large range of Mach numbers (e.g. Mach 5–24) when they fueled with hydrogen. SCRAMjets satisfy shock–on–lip conditions by typically optimized at a selected design Mach number. At off–design speeds, a cowl door can be used to minimize air mass flow spillage. Cowl doors are generally scheduled open–loop. For a very flexible vehicle, however, feedback may be required in order to reduce sensitivity to modelling errors.

1.3.4.2. Vehicle Trajectories

Likely vehicle trajectories will lie within the so–called air–breathing corridor corresponding to dynamic pressures in the range $\bar{q} \in [500, 2000]$ psf where the lower bound is due to the lifting area limit and the upper bound is due to the structural limits. It should be noted that, SCRAMjet–powered vehicles will fly at the highest allowable dynamic pressure in order to maximize free–stream mass airflow per unit area to the engine, and accelerating vehicles would have to increase dynamic pressure in order to maintain mass flow per unit area to the engine Heiser et al. (1994b). In order to provide this reason, vehicle flying dynamic pressure range can be considered at $\bar{q} \in [1500, 1750]$ psf so that there is room to increase dynamic pressure by moving toward larger Mach numbers while avoiding thermal choking at the lower Mach numbers. From Heiser et al. (1994b) and figure 1.1, we can see that the air–breathing corridor is about 30 kft wide vertically. We can see that via a simple algebraic calculation if the flight path angle (FPA) deviates by about 2.86^{o} for 30 seconds at Mach 10 when the vehicle is flying along the center of the corridor, then the vehicle will leave the corridor. This unacceptable scenario illustrates the importance of FPA control, particularly, in the presence of uncertain flexible modes.

1.3.5. Aero–Propulsion Coupling

HSVs are uniquely characterized by unprecedented aero–propulsion coupling because of the strong coupling that is provided by the components between the lift, propulsion and volume Anderson (2006). As a result of this structure, we can consider the following situations.

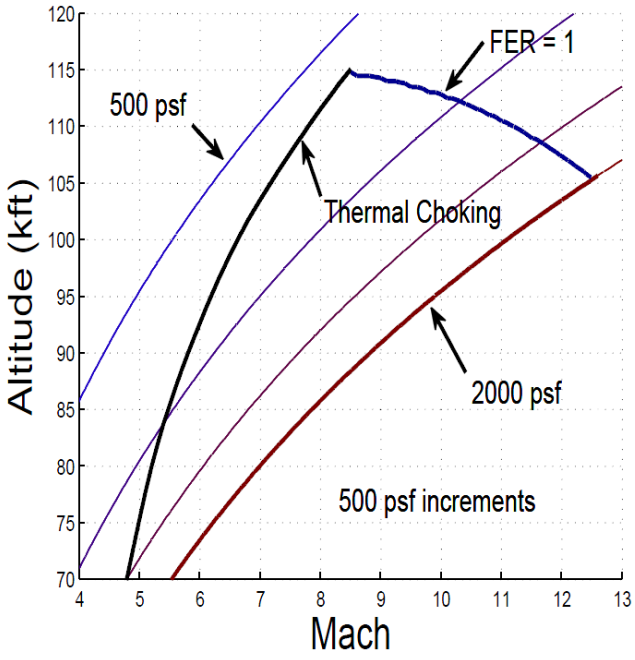

Figure 1.1. Air–Breathing Corridor, Dynamic Pressure, Thermal Choking and FER Constraints

- Since the external forebody and nozzle surfaces are parts of the engine flowpath Cockrell et al. (2002) aero performance cannot be decoupled from the engine performance.
- Vehicle aerodynamic properties affect the bow shock – detached for blunt leading edges, attached for sharp leading edges. This influences the engine inlet conditions which, in turn, influences thrust, lift, drag, external nozzle conditions, and pitching moment.

Finally, it must be noted that SCRAMjet air mass capture area, spillage, engine performance, as well as overall vehicle stability and control properties depend upon velocity, AoA, side–slip–angle (SSA), and engine power setting.

1.3.6. Hypersonic Flow Phenomena

Hypersonic flow is characterized by specific physical variables that become more dominating with increasing Mach number Anderson (2006), Bertin (1994), Bertin et al. (1992). For example, a boundary layer increases in direct proportion to the square of the Mach number and as a result of this, the body to appear thicker than it really is and this

situation affects pressure distribution, lift, drag, stability, skin friction, and heat transfer. And also shock layer variability is observed at around Mach 3 Anderson (2006).

1.3.7. Aerothermoelastic Propulsion

HSVs are generally unstable because of their structure (e.g. long forebody, rearward engine) Bolender and Doman (2007a); Chavez and Schmidt (1994). And also, such vehicles require a minimum control bandwith for stabilization Bolender and Doman (2007a); Stien (2003); Rodriguez (2004). However, flexible structural dynamics, actuator dynamics, right half plane zeros (*i.e.* non–minimum phase dynamics), other high frequency dynamic uncertainties and variable limits (e.g. control saturation level, temperature profile) can limit the bandwith. High Mach numbers can result in high temperature that will make the forebody more flexible. Bow shock wave and engine inlet oscillations can be considered among the results of this situation and also this can affect the available thrust, stability, and achievable performance. This situation can be a major control problem if the vehicle is too flexible and open loop unstable, so thermal protection system is important to reduce the heat–induced flexibility Bolender and Doman (2006); Williams et al. (2006a); Glass (2008); Marshall et al. (2005).

1.3.8. High Temperature Gas Effects

Caloric imperfection, vibrational excitation, O_2 dissociation, N_2 dissociation, radiation, rarefied gas effects can be considered as a high temperature gas effects Heiser et al. (1994b); Anderson (2006). The above hypersonic phenomena can accurately modelled by suitable partial differential equations. This situation highlights the relevant modelling and control challenges with the above interactions and associated uncertainty.

1.4. Contributions

In this thesis, modelling and control of HSVs are discussed. Firstly, the contributions to the modelling of HSVs is highlighted, next novelties of the proposed controller are presented.

In the HSV literature, there are several modelling works. Specifically, Bolender is the leading researcher of NASA in deriving dynamic models for HSV. While his works are widely acknowledgedi review of his HSV modelling papers and other relevant literature highlights the fact that none of the publicy distributed HSV models are complete in the sense that the model parameters are not published. Out attepmts to reach a complete HSV dynamic model were answered by the confidentiality restriction imposed by the sponsoring agencies (such as NASA, DARPA, US DoD, US AF, AFRL etc.).

Motivated by the lack of publicy available HSV dynamic models, in the earlier stages, all the available modelling approaches are investigated and a full nonlinear HSV dynamic model is obtained. While this nonlinear model can be used for numerically simulating the HSV dynamics, it is not control friendly in the sense that the control inputs can not be integrated to dynamic model directly. As a result, linearization techniques are employed to obtain the LPV model which includes linear terms along with a nonlinear distrubance–like term.

Comparing with the HSV modelling literature, our main contribution is to obtain a nonlinear HSV model and a LPV model *completely*.

Next, control of HSV is discussed. Given the highly complicated nature of the HSV dynamics and to compensate for the possible mismatches between the exact nonlinear and the partially linearized LPV model, robust control seems to be the only choice. During the error system development matrix decomposition method is utilized to deal with an uncertain non–symmetric and indefinite input gain a matrix. After this decomposition, a nonlinear controller which can alternatively be seen as a modified linear (*i.e*, PI) controller fused with integral of the signum of the error terms for uncertainty compensation. The stability of the closed–loop system is investigated via Lyapunov–based arguments, and exponential stability of the tracking error is ensured when compared with the existing literature on control of HSVs a novel robust controller is proposed and as a result of the nature of the Lyapunov–type stability analysis, the proposed controller is *provably correct*.

1.5. Outline

The rest of this thesis is organized as follows. Chapter 2 summarized the modelling approach of the HSV and describes the mathematical models of the longitudinal dynamics of the HSVs. Chapter 3 describes control oriented modelling and summarizes some 3 DoF control models that are widely used in the literature. In Chapter 4, a novel,

nonlinear Lyapunov–based robust controller designed for LPV model of HSVs, is presented. Chapter 5 describes Matlab Simulink model of the system and numerical simulation results of the designed controller. Finally, Chapter 6 summarizes the result of this thesis, and suggests possible directions for future research.

CHAPTER 2

OVERVIEW OF THE HYPERSONIC VEHICLE MODEL

In this chapter, we consider the nonlinear 3 DoF dynamical model for the longitudinal dynamics of a generic SCRAMjet–powered HSV developed by Bolender and Doman (2005), Bolender and Doman (2007a), Bolender and Doman (2006), Williams et al. (2006a) ,Sigthorsson et al. (2006), Groves et al. (2005), Groves et al. (2006), Bolender et al. (2007), Parker et al. (2007), Oppenheimer et al. (2007), Doman et al. (2006), Adami et al. (2006), Parker et al. (2005).

The model associated with the vehicle is assumed to be made of titanium. It is 100 ft long with weight 6,154 lb per foot of depth and has a bending mode at about 21 rad/sec. The control inputs usually include elevator, stoichiometrically normalized fuel equivalence ratio (FER), canard, and a diffuser area ratio. However, in this thesis, we considered the case where elevator, FER and canard as the control inputs, and not considered diffuser area ratio. The vehicle may be visualized as shown in Figure 2.1 Bolender et al. (2007). Nominal model parameter values for the HSV are given in Table 2.1.

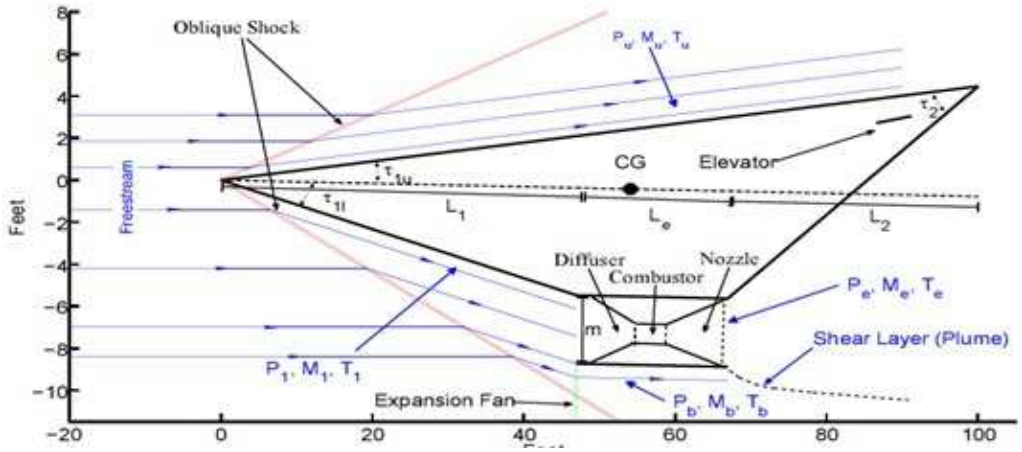

Figure 2.1. Schematic of a SCRAMjet–powered HSV Bolender et al. (2007)

Table 2.1. Nominal Values of the Vehicle Parameters

Parameter	Nominal Value
Total Length (L_T)	100 ft
Forebody Length (L_1)	47 ft
Aftbody Length (L_2)	33 ft
Engine Length	20 ft
Engine Inlet Height (h_i)	3.25 ft
Upper Forebody Angle (τ_{1U})	3 deg
Elevator Position	(-85, -3.5) ft
Diffuser Exit/Inlet Area Ratio	1
Titanium Thickness	9.6 in
First Flexible Mode (ω_{n1})	21.02 rad/s
Second Flexible Mode (ω_{n2})	101.00 rad/s
Third Flexible Mode (ω_{n3})	6.2 deg
Lower Forebody Angle (τ_{1L})	14.342 deg
Tail Angle (τ_2)	191.3 (slugs/ft)
Mass Per Unit Width	6154.1 lbs/ft
Weight Per Unit Width	8.6482 $\times 10^7$ psi
Mean Elasticity Modulus	86723 (slugs$\times$ft)
Moment of Inertia (I_{yy})	(-55,0) ft
Center of Gravity	17 ft^2
Elevator Area	6.35 ft^2
Nozzle Exit–to–Inlet Area Ratio	$50.87 rad/s$
Flexible Mode Damping (ξ)	0.02

2.1. Modelling Approach

In this section, we will briefly refer to the basic concepts of modelling under the main headings to make the modelling approach more tractable. We would like to highlight that modelling HSV is still an open research area and there are several internal and external effects that can be considered as parts of modelling. The main effects will be examined under in the following subsections.

2.1.1. Aerodynamics

In this subsection, we try to summarize the aerodynamic modelling approach which constitutes the main parts of the environmental modelling. Since the aerodynamic effects have a direct impact on the flight, they can be seen as not only the most important external factors but also the main environmental effects. Aerodynamic parameters must

be used during the calculation of several characteristic flight parameters (e.g. Mach number, dynamic pressure, external forces).Because of the above mentioned circumstances, it can easily be said that aerodynamic modelling is one of major parts of the HSV modelling approach.

The main specifications of the aerodynamic modelling can be summarized as follows.

- Pressure distributions are computed using inviscid compressible oblique–shock and Prandtl–Meyer expansion theory Bolender and Doman (2005); Anderson (2006); Bertin (1994); Anderson (2002).
- Air is assumed to be calorically perfect; *i.e.* constant specific heat and specific heat ratio $\gamma = \frac{C_p}{C_v} = 1.4$ Anderson (2006).
- A standard atmosphere model is used.
- Viscous drag effects (*i.e.* an analytical skin friction model) are captured using Eckert's temperature reference method Bolender et al. (2007); Anderson (2006). This relies on using the incompressible turbulent skin friction coefficient formula for a flat plate at a reference temperature.
- Unsteady effects due to rotation and flexing are captured using linear piston theory Bolender et al. (2007); Oppenheimer and Doman (2006b). The linear piston theory utilizes the fact that flow velocities induce pressures just as the pressure exerted by a piston on a fluid induces a velocity Oppenheimer and Doman (2006a).

2.1.2. Propulsion

In this subsection, we try to summarize the propulsion modelling approach which is necessary for integrating SCRAMjet engine technology effects to the dynamical model. As mentioned before, a special engine technology, namely as SCRAMjet, is used at HSVs.Since the propulsion effects of this engine technology is more different and stronger than most of the other engine technologies, flight parameters are affected by these effects more dramatically. It is very important that to obtain a good propulsion modelling to capture these effects.

The model assumes the presence of an infinitely fast cowl door which AoA to achieve shock–on–lip conditions (assuming no forebody flexing – *i.e.*, flight total angle

(FTA) is precisely known). Forebody flexing, however, results in air mass flow spillage Bolender and Doman (2005). At the cruise condition design, the bow shock impinges on the engine inlet (assuming no flexing). At speeds below the design–flight condition and/or larger flow turning angles, the shock angle is large and the cowl moves forward to capture the shock. At larger speeds and/or smaller flow turning angles, the shock angle is small and the bow shock is absorbed by the engine. In either case, there is a shock reflected from the cowl or within the inlet. This reflected shock further slows down the flow and steers it into the engine.

It should be noted that shock–shock interactions are not modelled. For example, at larger speeds and smaller flow turning angles, there is a shock of the inlet lip. This shock interacts with the bow shock. This interaction is not captured in the model (such interactions are discussed in Anderson (2006)).

HSVs use liquid hydrogen (LH_2) as the fuel. It is commonly assumed that fuel mass flow is negligible compared to the air mass flow. Thrust is linearly related to FER for all expected FER values. For large FER values, the thrust levels off. In practice, when FER is greater than 1, this results in decreased thrust. This phenomena Bolender and Doman (2005) is not captured in the model. As such, control designs based on this nonlinear model (or derived linear models) should try to maintain FER below unity.

2.1.3. Structural

In this subsection, we try to summarize the structural modelling approach which constitutes the main parts of HSV dynamical model with its calculated parameters. They are used for several calculations including the natural frequencies and modes shapes for the flexible states.

The main specifications of the structural modelling can be summarized as follows.

- A single free–free Euler–Bernoulli beam partial differential equation (infinite dimensional partial differential equation) model is used to capture vehicle longitudinal elasticity. As such, out–of–plane loading, torsion, and Timoshenko effects are neglected.

- The assumed modes method (based on a global basis) is used to obtain natural frequencies, mode shapes, and finite–dimensional approximate values. This results in a model whereby the rigid body dynamics influence the flexible dynamics through the generalized forces Williams et al. (2006a).

- This is in contrast to the model described within Bolender and Doman (2005) which uses fore and aft cantilever beams (clamped at the center of gravity) and leads to the rigid body modes being inertially coupled to the flexible modes (*i.e.* rigid body modes directly excite flexible modes). Within the current model, the forebody deflection (a function of the generalized forces N_i) influences the rigid body dynamics via the bow shock which influences engine inlet conditions, thrust, lift, drag, and moment Williams et al. (2006a). Aftbody deflections influence the AoA seen by the elevator. As such, the flexible modes influence the rigid body dynamics as well.

2.1.4. Actuator Dynamics

Simple first order actuator models (contained within the original model) were used in each of the control channels: elevator–$\frac{20}{s+20}$, FER–$\frac{10}{s+10}$, canard–$\frac{20}{s+20}$. These dynamics did not prove to be critical in our study. An elevator saturation of $\pm 30^{\text{o}}$ was used Sigthorsson et al. (2006); Groves et al. (2006). It should be noted that these limits were never reached in our studies like the past studies which include Soloway et al. (2009); Dickeson et al. (2009); Rodriguez et al. (2009).

A saturation level–associated with FER (e.g. thermal choking and unity FER)–was also directly addressed Groves et al. (2005). Generally speaking, the vehicle exhibits unstable non–minimum phase dynamics with nonlinear aero–elastic–propulsion coupling and critical FER constraints.

2.2. Unmodelled Phenomena/Effects

All models possess fundamental limitations. Realizing model limitations is crucial in order to avoid misuse of the developed model. Given this, we now provide a (somewhat lengthy) list of phenomena/effects that are not captured during the modelling of HSV.

2.2.1. Dynamics

The 3 DoF nonlinear model does not capture longitudinal–lateral coupling and dynamics associated with 6 DoF effects.

2.2.2. Aerodynamics

Aerodynamic phenomena/effects not captured in the model include the following: boundary layer growth, displacement thickness, viscous interaction, entropy and vorticity effects, laminar versus turbulent flow, flow separation, high temperature and real gas effects (e.g. caloric imperfection, electronic excitation, thermal imperfection, chemical reactions such as O_2 dissociation), non–standard atmosphere (e.g. troposphere, stratosphere), unsteady atmospheric effects, 3D effects, aerodynamic load limits.

2.2.3. Propulsion

Propulsion phenomena/effects not captured in the model include the following: cowl door dynamics, multiple forebody compression ramps (for example there are three of them on X–43A Berry et al. (2008, 2001)), forebody boundary layer transition and turbulent flow to inlet Berry et al. (2008, 2001), diffuser losses, shock interactions, internal shock effects, diffuser combustor interactions, fuel injection and mixing, flame holding, engine ignition via pyrophoric silane McClinton (2007) (requires finite–rate chemistry; cannot be predicted via equilibrium methods Starkey et al. (2008)), finite–rate chemistry and the associated thrust–AoA–Mach–FER sensitivity effects Baldelli et al. (2005), internal and external nozzle losses, thermal choking induced phenomena (2D and 3D) and unstart, exhaust plume characteristics, combined cycle issues Heiser et al. (1994a).

2.2.4. Structural

Structural phenomena/effects not captured in the model include the following: out of plane and torsional effects, internal structural layout, unsteady thermoelastic heating effects, aerodynamic heating due to shock impingement, distinct material properties Glass (2008), and aero–servo–elasticity Baldelli et al. (2005); Lind and Brenner (1999).

2.3. Equations of Motion

The equations of motion for the 3 DoF flexible hypersonic vehicle are given as follows Williams et al. (2006b):

$$\dot{v} = \left[\frac{Tcos\alpha - D}{m}\right] - gsin\gamma \tag{2.1}$$

$$\dot{\alpha} = -\left[\frac{L + Tsin\alpha}{mv}\right] + q + \left[\frac{g}{v} - \frac{v}{R_E + h}\right] cos\gamma \tag{2.2}$$

$$\dot{q} = \frac{M}{I_{yy}} \tag{2.3}$$

$$\dot{h} = vsin\gamma \tag{2.4}$$

$$\dot{\theta} = q \tag{2.5}$$

$$\ddot{\eta}_i = -2\xi\omega_i\dot{\eta}_i - \omega_i^2\eta_i + N_i,\ i = 1,\ 2,\ 3 \tag{2.6}$$

$$\gamma \triangleq \theta - \alpha \tag{2.7}$$

$$g = g_0\left[\frac{R_E}{R_E + h}\right]^2 \tag{2.8}$$

where L denotes lift, T denotes engine thrust, D denotes drag, M is the pitching moment, N_i denotes generalized forces, ξ_i denotes flexible mode damping factor, ω_i denotes flexible mode undamped natural frequencies, m denotes the vehicle's total mass, I_{yy} is the pitch axis moment of inertia, g_0 is the acceleration due to gravity at sea level, and R_E is the radius of the Earth.

The states consist of five classical rigid body states and six flexible modes states where the rigid states are velocity v, AoA α, pitch rate q, altitude h, pitch angle θ, and the flexible body states are $\eta_1,\ \dot{\eta}_1,\ \eta_2,\ \dot{\eta}_2,\ \eta_3,\ \dot{\eta}_3$. These eleven states are summarized in Table 2.2.

State variables are combined in a vector denoted by $x\,(t) \in \mathbb{R}^{11}$, and is defined as

$$x \triangleq \begin{bmatrix} x_{RB}^T & x_F^T \end{bmatrix}^T. \tag{2.9}$$

The vehicle has three control inputs: FER, a rearward situated elevator δ_e and a forward situated canard δ_c. These control inputs are summarized in Table 2.3.

2.4. Force and Moment Summations

While the equations of motion in (2.1) – (2.6) apply to almost any 3 DoF aircraft, the force and moment summations Lift, Drag, Thrust, Moment, and generalized forces

Table 2.2. States of Hypersonic Vehicle Model

#	Symbol	Description	Units
1	v	Velocity	ft/sec
2	α	Angle of Attack (AoA)	deg
3	q	Pitch Rate	deg/sec
4	h	Altitude	ft
5	θ	Pitch Angle	deg
6	η_1	1^{st} flexible mode	-
7	$\dot{\eta}_1$	1^{st} flexible mode rate	1/sec
8	η_2	2^{nd} flexible mode	-
9	$\dot{\eta}_2$	2^{nd} flexible mode rate	1/sec
10	η_3	3^{rd} flexible mode	-
11	$\dot{\eta}_3$	3^{rd} flexible mode rate	1/sec

Table 2.3. Controls of Hypersonic Vehicle Model

#	Symbol	Description	Units
1	*FER*	Stoichiometrically Normalized Fuel Equivalence Ratio	-
2	δ_e	Elevator Deflection	deg
3	δ_c	Canard Deflection	deg

N_i for $i = 1, 2, 3$, are specific to the SCRAMjet–powered HSV and can be obtained via the following expressions. These forces and moments are comprised of the breakdown of pressures in the body x and z directions. The equations for these forces and moments are Bolender and Doman (2005):

$$L = F_x \sin(\alpha) - F_z \cos(\alpha) + \text{Lift}_{\text{viscous}} \tag{2.10}$$

$$D = -(F_x \cos(\alpha) - F_z \sin(\alpha)) + \text{Drag}_{\text{viscous}} \tag{2.11}$$

$$T = \dot{m}_a (V_e - V_\infty) + (p_e - p_\infty) A_e \tag{2.12}$$

$$M = M_f + M_e + M_{\text{inlet}} + M_{cs} + M_u + M_b + M_{\text{unsteady}} \left(L_1 \tan(\tau_{1l}) \frac{h_i}{2} - cg \right) \text{Thrust} + M_{\text{viscous}} \tag{2.13}$$

$$N_i = \int p(x,t)\, \partial i(x)\, dx + \sum_j F_j(t) \partial i(x_j) \tag{2.14}$$

where V_e is the speed of flow exiting the engine, V_∞ is the freestream speed, p_e is the pressure at the exit of the internal nozzle, p_∞ is freestream pressure, $\dot{m}_a$ is the mass airflow into the engine, A_e is engine exit area per unit span, F_x and F_z are the sum of

Table 2.4. Forces and Moments

Symbol	Description
N_i	i^{th} generalized force
F_j	j^{th} point load acting at point x_j on the vehicle
F_x, F_z	sum of forces in x and z direction
$Lift_{viscous}$	lift due to viscous effects
$Drag_{viscous}$	drag due to viscous effects
$F_{x,f}$, $F_{z,f}$	lower forebody forces, x and z direction
$F_{x,u}$, $F_{z,u}$	upper forebody forces, x and z direction
$F_{x,inlet}$, $F_{z,inlet}$	forces in the engine inlet, x and z direction
$F_{x,e}$, $F_{z,e}$	exhaust forces on aftbody, x and z direction
$F_{x,cs}$, $F_{z,cs}$	elevator forces, x and z direction
$F_{x,unsteady}$, $F_{z,unsteady}$	unsteady forces, x and z direction
$F_{z,b}$	pressure on bottom of vehicle, z direction
$M_{unsteady}$	moment due to unsteady pressure distribution
$M_{viscous}$	moment due to viscous effects
M_f	moment due to lower forebody forces
M_u	moment due to upper forebody forces
M_{inlet}	moment due to turning force at engine inlet
M_{cs}	moment due to control surface forces
M_b	moment due to engine base force

forces in the x and z directions, respectively, and α is the AoA of the vehicle. The forces and moments are summarized in Table 2.4

CHAPTER 3

CONTROL ORIENTED MODELLING

It is obvious that HSV dynamic model doesn't relate with control inputs directly. Since the common main objective is to control the system, the control inputs must be integrated into the dynamic model efficiently. Control oriented modelling approach which is determining the aerodynamic forces and moments equations in terms of the control inputs by curve fitting approximation is very useful to achieve this goal. In this section we will explain this curve fitting approximation along with the LPV approach which constructs the basis for our controller design.

3.1. Control Design Model

In this subsection, control design model of the HSV is considered which relates the equations of motion in (2.1) – (2.6) and the control inputs (given in Table 2.3).

There are two control design model available in the literature up to now. The first control design model which is widely used in past works and doesn't include the flexible states. This control design model can be adopted in the control design with reduced control authority only, while the second control design model, which is widely used in the last decade, can be used in the control design with full control authority. Similar to Parker et al. (2007), the second control design model has been derived using curve fitted approximations of the aerodynamic and propulsive forces. In contrast to Parker et al. (2007), however, this control oriented model retains the dominant features of equations of motion which are problematic for the control design, including non–minimum phase behavior of the flight path angle dynamics, flexibility effects, and coupling between the propulsion system and the airframe. Since the control design with minimal control authority presents a set of severe challenges, it is very difficult to obtain the second control design model from the first control design model by adding the flexible states, the altitude dynamics and some other couplings. Although the second control design model seems more difficult, it is widely used in the literature, and we preferred to utilized in this thesis mostly because of it is a better approximation of the highly nonlinear HSV dynamics. Aside from this, we also considered the fact that the Hypersonic flights are extremely affected from the

flexible states in practice and these flexible states should be considered when obtaining an accurate HSV dynamical model. After this point, we will explain this control design model. In the equations of motion given in (2.1)–(2.6), the relationships between the control inputs and controlled outputs do not admit a closed–form representation. Following the approach used in Parker et al. (2007), a simplified model has been derived for control design and stability analysis.

This model, referred to as the control design model Bolender and Doman (2005), approximates the behavior of the equations of motion by replacing the aerodynamic and generalized forces and moments with curve–fitted functions of the rigid body states, the control inputs and the elastic modes. The resulting nonlinear model, albeit still quite complex, offers the advantage of being analytically tractable, while retaining the relevant dynamical features of the equations of motion. The approximations of the forces and moments are given as follows

$$T \approx \overline{q}S\left[C_{T,FER}\left(\alpha\right)FER + C_T\left(\alpha\right) + C_T^{\eta}\eta\right] \tag{3.1}$$

$$L \approx \overline{q}SC_L(\alpha,\delta,\eta) \tag{3.2}$$

$$D \approx \overline{q}SC_D(\alpha,\delta,\eta) \tag{3.3}$$

$$M \approx z_T T + \overline{qc}SC_M(\alpha,\delta,\eta) \tag{3.4}$$

$$N_i \approx \overline{q}S\left[N_i^{\alpha^2}\alpha^2 + N_i^{\alpha}\alpha + N_i^{\delta_e}\delta_e + N_i^{\delta_c}\delta_c + N_i^0 + N_i^{\eta}\eta\right] \quad i = 1,2,3 \tag{3.5}$$

where $\delta = \left[\delta_e,\ \delta_c\right]^T$ and

$$C_{T,FER}\left(\alpha\right) = C_T^{FER\alpha^3}\alpha^3 + C_T^{FER\alpha^2}\alpha^2 + C_T^{FER\alpha}\alpha + C_T^{FER} \tag{3.6}$$

$$C_T\left(\alpha\right) = C_T^3\alpha^3 + C_T^2\alpha^2 + C_T^1\alpha + C_T^0 \tag{3.7}$$

$$C_M\left(\alpha,\delta,\eta\right) = C_M^{\alpha^2}\alpha^2 + C_M^{\alpha}\alpha + C_M^{\delta_e}\delta_e + C_M^{\delta_c}\delta_c + C_M^0 + C_M^{\eta}\eta \tag{3.8}$$

$$C_L\left(\alpha,\delta,\eta\right) = C_L^{\alpha}\alpha + C_L^{\delta_e}\delta_e + C_L^{\delta_c}\delta_c + C_L^0 + C_L^{\eta}\eta \tag{3.9}$$

$$\begin{aligned} C_D\left(\alpha,\delta,\eta\right) = {} & C_D^{\alpha^2}\alpha^2 + C_D^{\alpha}\alpha + C_D^{{\delta_e}^2}{\delta_e}^2 + C_D^{\delta_e}\delta_e \\ & C_D^{{\delta_c}^2}{\delta_c}^2 + C_D^{\delta_c}\delta_c + C_D^0 + C_D^{\eta}\eta \end{aligned} \tag{3.10}$$

$$C_j^{\eta} = \left[\begin{array}{cccccc} C_j^{\eta_1} & 0 & C_j^{\eta_2} & 0 & C_j^{\eta_3} & 0 \end{array}\right],\ j = T,\ M,\ L,\ D \tag{3.11}$$

$$N_i^{\eta} = \left[\begin{array}{cccccc} N_i^{\eta_1} & 0 & N_i^{\eta_2} & 0 & N_i^{\eta_3} & 0 \end{array}\right],\ i = 1,\ 2,\ 3 \tag{3.12}$$

$$\eta = \left[\begin{array}{cccccc} \eta_1 & \dot{\eta}_1 & \eta_2 & \dot{\eta}_2 & \eta_3 & \dot{\eta}_3 \end{array}\right]^T \tag{3.13}$$

where $C_T^{(.)},\ C_M^{(.)}, C_L^{(.)}, C_D^{(.)}$ are constant coefficients, $\overline{c}$ denotes constant mean aerodynamic chord, S and z_T denotes constant reference area and constant thrust–to–moment coupling coefficient, respectively, $\overline{q}$ denotes dynamic pressure and is expressed as

$$\overline{q} = \frac{1}{2}\rho V^2 \tag{3.14}$$

where $\rho(\cdot) \in \mathbb{R}$ denotes the density and $V(\cdot) \in \mathbb{R}$ denotes the velocity.

Since control design model has been obtained from a curve–fitted approximation of a 3 DoF nonlinear HSV model, it is essential that the control law provides robustness with respect to uncertainty in the plant model parameters.

3.1.1. Linear Parameter Varying Approach

Linearization is a very popular approach to facilitate the control design and the analysis of closed–loop HSV dynamics. There are two commonly utilized linearization approaches available in the HSV literature. The first approach, which results in a dynamic model that is entirely linear, is the most popular one and widely used in HSV works. Despite simplifying the control design, it doesn't provide a good approximation and can't be used for all situations. The second approach, which is known as the LPV approach and provides a better approximation to the real HSV model.

In contrast to the fully linearized model, the LPV model is partially linearized. In addition to constant nominal state and input matrices and the constant output matrix, it contains some time–dependent weighting terms which can be used for capture the time–dependent nature of the 3 DoF *real* nonlinear model. Additionally some unmodelled effects and disturbances can be considered in this model by using a nonlinear disturbance–like function.

To facilitate the subsequent control development, dynamic model is rearranged as a combination of LPV matrices with nonlinearity caused from unmodelled effects as

$$\dot{x} = A(\rho(t))\,x + B(\rho(t))\,u + f(t) \tag{3.15}$$

$$y = Cx \tag{3.16}$$

where $A(\rho(t)) \in \mathbb{R}^{11\times 11}$ denotes a LPV state matrix, $B(\rho(t)) \in \mathbb{R}^{11\times p}$ denotes a column deficient LPV input matrix, $C \in \mathbb{R}^{p\times 11}$ denotes a known output matrix, $u(t) \in \mathbb{R}^{p}$ denotes a vector of p control inputs, $\rho(t)$ represents the unknown time dependent temperature profile of the aircraft, and $f(t) \in \mathbb{R}^{11}$ represents a time dependent unknown nonlinear disturbance–like function caused by the unmodelled effects.

The matrices $A(\rho(t))$ and $B(\rho(t))$ have standard LPV form Wilcox et al. (2010a);

Bhat (2008); Wilcox (2010):

$$A\left(\rho\left(t\right)\right) = A_0 + \sum_{i=1}^{s} w_i(\rho(t))A_i \tag{3.17}$$

$$B\left(\rho\left(t\right)\right) = B_0 + \sum_{i=1}^{s} v_i(\rho(t))B_i \tag{3.18}$$

where $A_0 \in \mathbb{R}^{11\times 11}$ and $B_0 \in \mathbb{R}^{11\times p}$ represents known nominal matrices with unknown variations $w_i(\rho(t))A_i$ and $v_i\left(\rho\left(t\right)\right)B_i$ are parameter dependent weighting terms.

In developing the controller and assessing its closed–loop performance, it is assumed that all of the coefficients of control design model are subject to uncertainty, apart from obvious parameters corresponding to physically measurable quantities or known constants.

CHAPTER 4

CONTROLLER DESIGN AND ANALYSIS

In this chapter, we will give detailed information our Lyapunov–based robust nonlinear controller that was deigned by using LPV approach.

4.1. Introduction

Any realistic HSV model includes nonlinearities and highly–coupled dynamics to provide a better approximation to the real system. For example, the aerodynamic properties are affected from the structural dynamics. While vibration in the forward fuselage changes the apparent turn angle of the flow, which results in changes in the pressure distribution over the forebody of the aircraft. The resulting changes in the pressure distribution over the aircraft manifest themselves as thrust, lift, drag, and pitching moment perturbations Bolender and Doman (2007b). On the other hand, aerothermoelastic effects, which are the response of elastic structures to aerodynamic heating and loading, cannot be ignored in hypersonic flight simply because such effects can destabilize the HSV system Heeg et al. (1993); Wilcox (2010). Also a loss of stiffness induced by aerodynamic heating has been shown to potentially induce dynamic instability in supersonic/hypersonic flight speed regimes Abbasa et al. (2008). As a result of their extremely complex and highly coupled dynamic models, control of HSVs is an important and challenging open problem. And control laws aiming to control longitudinal dynamics of an HSV should be capable of compensating for these structural and aerothermoelastic effects, structural temperature variations and structural dynamics must be considered Wilcox (2010).

To specifically deal with some of these dynamic–related uncertainties, some control algorithms were proposed. Active control was utilized to expand the flutter boundary and to convert unstable limit cycle oscillations (LCO) to stable ones Abbasa et al. (2008). An active structural controller was developed by Lind (2001), which accounts for variations in the HSV structural properties resulting from aerothermoelastic effects. The control design Lind (2001) models the structural dynamics using a LPV framework, and states the benefits of using the LPV framework as: the dynamics can be represented as a single model, and controllers can be designed that have affine dependency on the

operating parameters.

Some other past research have examined the challenges associated with control of HSVs. For example, HSV flight controllers were designed using genetic algorithms to search a design parameter space where the nonlinear longitudinal equations of motion contained uncertain parameters Austin and Jacobs (2001), Marrison and Stengel (1998), Wang and Stengel (2000). Some of these designs such as Baumann et al. (2008) utilized Monte Carlo simulations to estimate system robustness at each search iteration. Another approach by Austin and Jacobs (2001) utilized fuzzy logic to control the attitude of the HSV about a single low end flight condition. While such approaches Austin and Jacobs (2001), Marrison and Stengel (1998), Wang and Stengel (2000) generate stabilizing controllers, the procedures were computationally demanding and required multiple evaluation simulations of the objective function and have large convergence times.

Some of the early control laws were either linear or utilized feedback linearization to obtain a simple linearized model from the nonlinear HSV model. Sigthorsson et al. (2008) designed linear output feedback tracking control methods, where sensor placement strategies can be used to increase observability, or reconstruct full state information for a state–feedback controller. Feedback linearization techniques have also been applied to a control oriented HSV model to design a nonlinear controller Parker et al. (2007) where the model in Parker et al. (2007) was based on a previously developed by Bolender and Doman (2005) HSV longitudinal dynamic model. The control design by Parker et al. (2007) neglects variations in thrust lift parameters, altitude, and dynamic pressure.

Focus of some other past research was designing control laws to deal with structured and unstructured uncertainties. A robust output feedback technique was also developed for the linear parameterizable HSV model, which does not rely on state observation Sigthorsson et al. (2008). A robust set point regulation controller is designed to yield asymptotic regulation for a linearly parameterizable HSV model in the presence of parametric and structural uncertainties Fiorentini et al. (2007). Yoshihiko (2003) designed an adaptive gain–scheduled controller by using estimates of the scheduled parameters, and a semi–optimal controller was developed to adaptively attain H_∞ control performance. This controller yielded uniformly bounded stability due to the effects of approximation errors and algorithmic errors in the neural networks. An adaptive controller was designed to handle structured modelling uncertainties, actuator failures, and non–minimum phase dynamics for a HSV with elevator and FER inputs Gibson et al. (2009). Another adaptive approach Serrani et al. (2009) was recently developed with the addition of a guidance law that maintains the fuel ratio within its choking limits. While robust or adaptive control

and guidance control strategies for an HSV were investigated Fiorentini et al. (2007), Gibson et al. (2009), Serrani et al. (2009), neither of these works addressed the case where dynamics include uncertain disturbances. Review of the relevant highlighted the need for a continuous controller, which is capable of achieving exponential tracking for an HSV dynamic model containing aerothermoelastic effects and disturbances.

Recently in Wilcox et al. (2010b) and Wilcox (2010), a Lyapunov–based robust controller was proposed where it was claimed that exponential output tracking was ensured. While reading the paper, we noticed that the authors stated "As a result of a conservative stability analysis, the final gains used may **not satisfy the sufficient gain conditions** developed in the control development and the theorem proof provided in the stability analysis. The subsequent results indicate that the developed controller can be applied despite the fact that some gain conditions may not be satisfied." While, the above statement was acceptable from a control theoretic point of view, we decided to approach the paper with a mathematical rigor. A close investigation resulted in some questions regarding the choice of a parameter, namely ϵ, they introduced in Assumption 5. However, the authors did not provide the value of the parameter utilized in their numerical studies and thus we could neither verify nor disprove their result. This point was the starting point of this thesis.

Motivated by the lack of provably correct robust control algorithms for HSVs, we aimed to design a *provably correct* robust control law. We started with the same dynamic model, namely an LPV model, as in Wilcox et al. (2010b) and Wilcox (2010). The assumptions imposed on the model were similar, and same control objectives were aimed. Specifically, the main control objective was to ensure output tracking of a time–varying reference model output. After that point, our design followed a fundamentally different path than the one in Wilcox et al. (2010b) and Wilcox (2010). After designing the output tracking error and an auxiliary error signal, the open–loop error system was investigated. In the open–loop error system, the control input was multiplied with a partially unknown time–varying matrix. Neither symmetry nor positive definiteness of this unknown matrix could be investigated, which avoided it to be utilized as part of the Lyapunov function. When trying to deal with this unknown time–varying matrix, we decided to decompose it into a multiplication of a symmetric positive definite matrix, a diagonal matrix with its entries being $+1$ or -1, and a unity upper triangular matrix. Since, the original matrix was unknown, unfortunately, its decomposition was also unknown. However, we noticed that the symmetric positive definite matrix could be utilized as part of the Lyapunov function, and when this is the case, all we required was the knowledge of the diagonal matrix

with its entries being $+1$ or -1 that was also obtained via the decomposition. Provided the knowledge of this diagonal matrix, we designed a novel robust control law for HSVs. The stability of the closed–loop system is analyzed via Lyapunov–based arguments and exponential stability was ensured.

In the literature, the closest work to ours is Wilcox et al. (2010b) and Wilcox (2010), and comparing our results with theirs, we can confidently say that our controller is provably correct, while theirs have a weakness about the choice of a design parameter. Furthermore, their controller required the knowledge of the nominal value of the input gain matrix, while ours required the diagonal matrix obtained via the decomposition of an unknown time–varying matrix. While this seems like a restrictive assumption to impose, we decided to numerically apply the decomposition to our dynamic model and to some of the HSV models in the literature. This resulted in the diagonal matrix being equal to a standard identity matrix (*i.e.*, all its diagonal entries being equal to $+1$).

4.2. Control Development

In this section, we will introduced a nonlinear robust controller which is obtained for the using LPV model of HSV. This Lyapunov–based robust controller provides an exponential tracking performance and this situation is substantiated with detailed stability analysis.

4.2.1. Dynamic Model

The LPV model in (3.15) and (3.16) is utilized where the state and input matrices were defined in (3.17) and (3.18).

Assumption 1 *The dynamics given in* (3.15) *and* (3.16) *is assumed to be controllable. While the dynamic terms A, B and f are considered to be uncertain, the constant output matrix C is assumed to be known for this work. Furthermore, A, B, f and their first time derivatives are assumed to be bounded functions of time (i.e., A, B, f, $\dot{A}$, $\dot{B}$, $\dot{f} \in \mathcal{L}_\infty$).*

4.2.2. Control Objective

The control objective is to ensure that the output $y(t)$ tracks the time–varying reference output generated from the reference model given as

$$\dot{x}_m = A_m x_m + B_m \delta \tag{4.1}$$

$$y_m = C x_m \tag{4.2}$$

where $A_m \in \mathbb{R}^{11\times 11}$ and $B_m \in \mathbb{R}^{11\times p}$ denote constant state and input matrices, respectively, $\delta(t) \in \mathbb{R}^p$ is the reference input, $y_m(t) \in \mathbb{R}$ is the reference output, and C was defined in (3.16).

Assumption 2 *It is noted that, the state matrix A_m is chosen to be Hurwitz, and the reference input $\delta(t)$ and its first time derivative are assumed to be bounded (i.e., $\delta(t)$, $\dot{\delta}(t) \in \mathcal{L}_\infty$). This boundedness assumption permits linear signal chasing arguments to be utilized to prove that $x_m(t)$, $\dot{x}_m(t)$, $\ddot{x}_m(t)$, and thus $y_m(t)$, $\dot{y}_m(t)$, $\ddot{y}_m(t)$ are bounded functions of time.*

To quantify the tracking control objective, an output tracking error, denoted by $e(t) \in \mathbb{R}^p$, is defined as the difference between the outputs of the reference model and the HSV system

$$e \triangleq y - y_m \tag{4.3}$$

$$= C(x - x_m) \tag{4.4}$$

where (3.16) and (4.2) were utilized. To ease the presentation of the control development and the subsequent stability analysis, we now introduce an auxiliary error signal, denoted by $r(t) \in \mathbb{R}^p$, as

$$r \triangleq \dot{e} + \gamma e \tag{4.5}$$

where $\gamma \in \mathbb{R}^{p\times p}$ is a diagonal, positive definite constant gain matrix.

Assumption 3 *To facilitate the subsequent control development, the state vector $x(t)$ in* (3.15) *which was previously defined in* (2.9) *is considered to be partitioned as*

$$x = \overline{x} + x_u \tag{4.6}$$

where $\overline{x}(t) \in \mathbb{R}^{11}$ contains p output states and $x_u(t) \in \mathbb{R}^{11}$ contains the rest of the states.

It is assumed that $x_u(t)$ can be partitioned as

$$x_u = x_{\rho_u} + x_{\varsigma_u} \tag{4.7}$$

where $x_{\rho_u}(t)$, $x_{\varsigma_u}(t) \in \mathbb{R}^{11}$ *can be bounded as*

$$\|x_{\rho_u}(t)\| \leq c_1 \|z(t)\| \tag{4.8}$$

$$\|x_{\varsigma_u}(t)\| \leq \varsigma_{x_u} \tag{4.9}$$

where c_1, $\varsigma_{x_u} \in \mathbb{R}$ *are positive bounding constants and* $z(t) \in \mathbb{R}^{2p}$ *is the combined error signal defined as*

$$z \triangleq \begin{bmatrix} e^T & r^T \end{bmatrix}^T \tag{4.10}$$

with $\|\cdot\|$ *denoting the standard Euclidean norm. Similarly, from the time derivative of* (4.7)*, we can obtain*

$$\dot{x}_u = \dot{x}_{\rho_u} + \dot{x}_{\varsigma_u} \tag{4.11}$$

where the following bounds are obtained

$$\|\dot{x}_{\rho_u}(t)\| \leq c_2 \|z(t)\| \tag{4.12}$$

$$\|\dot{x}_{\varsigma_u}(t)\| \leq \varsigma_{\dot{x}_u} \tag{4.13}$$

where c_2, $\varsigma_{\dot{x}_u} \in \mathbb{R}$ *are positive bounding constants.*

4.2.3. Open–Loop Error System

After utilizing (3.15) and (4.1) along with (4.5), we can obtain

$$r = CAx + \Omega u + Cf - CA_m x_m - CB_m \delta + \gamma e \tag{4.14}$$

where $\Omega \triangleq CB \in \mathbb{R}^{p \times p}$.

At this point, we would like to recall that since B is uncertain then Ω is uncertain as well. To deal with problem, we will utilize the decomposition in Costa et al. (2003); Morse (1993); Tao (2003). Based on the structures of C and B, Ω is assumed to be a real matrix with non–zero leading principal minors. Based on this assumption, it can be decomposed as

$$\Omega = SD_D U \tag{4.15}$$

where $S(\rho(t))$, D_D, $U(\rho(t)) \in \mathbb{R}^{p \times p}$ are a positive definite symmetric matrix, a diagonal matrix with entries being ± 1, and a unity upper triangular matrix, respectively.

Remark The subsequent development requires D_D to be available (see Chen et al. (2008) for the precedence of this type of assumption). We would like to note that the structure

of some of the HSV dynamic models in the literature Fiorentini (2010), Korad (2010), Wilcox (2010), Williams et al. (2006b) were investigated for the validity of this assumption, and for the given model parameters the decomposition always yielded D_D to result in an identity matrix. We also would like to note that, due to the structure of dynamic model given in (3.15) and (3.16), the decomposition in (4.15) results in D_D to be an identity matrix. However the control development in this paper is aimed for the most general case where D_D may be any known $p \times p$ diagonal matrix with entries being $+1$ or -1.

After multiplying both sides of the time derivative of (4.14) with $S^{-1}(\rho(t))$, we can obtain

$$\begin{aligned} M_M \dot{r} &= M_M C \dot{A} x + M_M C A \dot{x} + D_D U \dot{u} + M_M C \dot{f} \\ &- M_M C A_m \dot{x}_m - M_M C B_m \dot{\delta} + \gamma M_M \dot{e} \\ &+ M_M C \dot{B} \Omega^{-1} (r - CAx - Cf + CA_m x_m + CB_m \delta - \gamma e) \end{aligned} \tag{4.16}$$

where $M_M(\rho(t)) \triangleq S^{-1} \in \mathbb{R}^{p \times p}$ is also symmetric and positive definite and satisfies the following inequalities

$$\underline{m} \|\mu\|^2 \leq \mu^T M_M(\rho(t)) \mu \leq \overline{m} \|\mu\|^2 \ \forall \mu \in \mathbb{R}^{p \times 1} \tag{4.17}$$

with $\underline{m}, \overline{m} \in \mathbb{R}$ being positive bounding constants.

To facilitate the error system development, an auxiliary signal, denoted by $N(x,t) \in \mathbb{R}^{p \times 1}$, is defined as

$$\begin{aligned} N \triangleq\ & M_M[C\dot{A}x + CA\dot{x} + C\dot{B}\Omega^{-1}(r - CAx - Cf + CA_m x_m + CB_m \delta + \gamma e) \\ & + C\dot{f} - CA_m \dot{x}_m - CB_m \dot{\delta} + \gamma \dot{e}] + e + \frac{1}{2} \dot{M}_M r. \end{aligned} \tag{4.18}$$

The idea behind the introduction of the auxiliary signal $N(x, \dot{x}, t)$ is to obtain two auxiliary terms after some straightforward algebraic manipulation. Specifically, the first term, denoted by $\overline{N}(\cdot) \triangleq N|_{x=x_m, \dot{x}=\dot{x}_m} \in \mathbb{R}^{p \times 1}$, contains bounded signals and is defined as

$$\begin{aligned} \overline{N} \triangleq\ & M_M[C\dot{A}x_m + CA\dot{x}_m + C\dot{B}\Omega^{-1}(-CAx_m - Cf + CA_m x_m + CB_m \delta) \\ & + C\dot{f} - CA_m \dot{x}_m - CB_m \dot{\delta}]. \end{aligned} \tag{4.19}$$

The second term, denoted by $\widetilde{N}(e, \dot{e}, r, t) \triangleq N - \overline{N} \in \mathbb{R}^{p \times 1}$, is an error–like signal obtained as

$$\begin{aligned} \widetilde{N} &= M_M C \dot{A}(x - x_m) + M_M CA(\dot{x} - \dot{x}_m) \\ &+ M_M C \dot{B} \Omega^{-1}(-CA(x - x_m) + r - \gamma e) \\ &+ M_M \gamma \dot{e} + e + \frac{1}{2} \dot{M}_M r \end{aligned} \tag{4.20}$$

where (4.18) and (4.19) were utilized. It is noted that, to facilitate the stability analysis, we will subsequently develop upper bounds for the auxiliary terms $\overline{N}$ and $\widetilde{N}$.

After utilizing the definitions in (4.18), (4.19), (4.20), the expression in (4.16) can be rewritten as

$$M_M \dot{r} = -\frac{1}{2}\dot{M}_M r - e - D_D U \dot{u} + \widetilde{N} + \overline{N}. \tag{4.21}$$

4.2.4. Closed–Loop Error System

Based on the open–loop error system in (4.21) and the subsequent stability analysis, the control input $u(t)$ is designed as

$$u(t) = D_D K \left[e(t) - e(t_0) + \gamma \int_{t_0}^{t} e(\sigma)\, d\sigma \right] + D_D \Pi \tag{4.22}$$

where $K \in \mathbb{R}^{p \times p}$ is a constant, positive definite, diagonal gain matrix and the auxiliary signal $\Pi(t) \in \mathbb{R}^{p \times 1}$ is updated according to

$$\dot{\Pi} = \beta \text{Sgn}(r), \Pi(t_0) = 0_p \tag{4.23}$$

where $0_p \in \mathbb{R}^{p \times 1}$ is a zero vector, $\beta \in \mathbb{R}^{p \times p}$ is a constant positive definite diagonal gain matrix and $\text{Sgn}(\cdot) \in \mathbb{R}^{p \times 1}$ is the vector signum function. Motivated by the subsequent analysis, the control gain matrix is chosen as

$$K = I_p + k_q I_p + \text{diag}\left\{k_{d,1}, \cdots, k_{d,(p-1)}, 0\right\} \tag{4.24}$$

where $k_q \in \mathbb{R}$ and $k_{d,i} \in \mathbb{R}$ $i = 1, \cdots, (p-1)$ are constant positive control gains. The time derivative of the control is obtained as

$$\dot{u} = D_D K r + D_D \beta \text{Sgn}(r) \tag{4.25}$$

where (4.5) and (4.23) were utilized. After substituting (4.25) into (4.21), and adding and subtracting Kr, the following closed–loop error system is obtained

$$M_M \dot{r} = -\frac{1}{2}\dot{M}_M r - e - Kr + \widetilde{N} + \overline{N} - D_D (U - I_p) D_D K r - D_D U D_D C \text{Sgn}(r) \tag{4.26}$$

where $I_p \in \mathbb{R}^{p \times p}$ is the standard identity matrix and the fact that $D_D D_D = I_p$ was utilized.

Before proceeding with the Lyapunov–based stability analysis, we would like to give more descriptive information about the last two terms of (4.26). After utilizing the fact that $(U - I_p)$ being strictly upper triangular, we can rewrite the term $D_D (U - I_p) D_D K r$ as

$$D_D (U - I_p) D_D K r = \begin{bmatrix} \Phi \\ 0 \end{bmatrix} \tag{4.27}$$

where $\Phi(t) \in \mathbb{R}^{(p-1)\times 1}$ is an auxiliary signal with its entries $\Phi_i(t) \in \mathbb{R}$, $i = 1, ..., (p-1)$, being defined as

$$\Phi_i \triangleq d_i \sum_{j=i+1}^{p} d_j k_j U_{i,j} r_j \tag{4.28}$$

where d_i is the i–th entry of D_D which is either $+1$ or -1, and k_i is the i–th entry of the control gain matrix K. Notice from the structure of the right–hand side of (4.27) that the last entry of the term $D_D(U - I_p) D_D K r$ is equal to 0, Φ_i depends on the $(i+1)$–th to p–th entries of the control gain matrix K. We can rewrite the $D_D U D_D \beta \text{Sgn}(r)$ term as

$$D_D U D_D \beta \text{Sgn}(r) = \begin{bmatrix} \Theta \\ 0 \end{bmatrix} + \beta \text{Sgn}(r) \tag{4.29}$$

where $\Theta(t) \in \mathbb{R}^{(p-1)\times 1}$ is an auxiliary signal with its entries $\Theta_i(t) \in \mathbb{R}$, $i = 1, \cdots, (p-1)$, being defined as

$$\Theta_i = d_i \sum_{j=i+1}^{p} d_j \beta_j U_{i,j} \text{sgn}(r_j) \tag{4.30}$$

where $\beta_i \in \mathbb{R}$ is the i–th entry of the control gain matrix β.

Remark The following upper bound can be obtained

$$\left\| \widetilde{N}(\cdot) \right\| \leq \rho_{\widetilde{N}} \|z\| \tag{4.31}$$

where $\rho_{\widetilde{N}}$ is a positive constant, and $z(t) \in \mathbb{R}$ was defined (4.10). Since the reference state and its time derivatives are bounded, it can be seen from (4.19) that the entries of $\overline{N}(t)$ are bounded in the sense that

$$\left| \overline{N}_i(t) \right| \leq \zeta_{\overline{N}_i} \tag{4.32}$$

where $\zeta_{\overline{N}_i} \in \mathbb{R}$ are positive bounding constants. Based on (4.28) and (4.30), following upper bounds can be obtained

$$|\Phi_i| \leq \sum_{j=i+1}^{p} k_j \zeta_{U_{i,j}} |r_j| \leq \zeta_{\Phi_i} \|z\| \tag{4.33}$$

$$|\Theta_i| \leq \sum_{j=i+1}^{p} \beta_j \zeta_{U_{i,j}} \leq \zeta_{\Theta_i} \tag{4.34}$$

where (4.10), (4.31) and (4.32) were utilized and $\zeta_{\Theta_i} \in \mathbb{R}$ is a positive bounding constant.

Proof The equation (4.20), can be upper bounded as

$$\begin{aligned}
\left\|\widetilde{N}\right\| &\leq \left\|M_M C\dot{A}C^+\right\|_{i_\infty} \|e\| \\
&+ \left\|M_M CAC^+\right\|_{i_\infty} \|\dot{e}\| \\
&+ \left\|M_M C\dot{B}\Omega^{-1}CAC^+\right\|_{i_\infty} \|e\| \\
&+ \left\|M_M C\dot{B}\Omega^{-1}\right\|_{i_\infty} \|r\| \\
&+ \left\|M_M C\dot{B}\Omega^{-1}\right\|_{i_\infty} \|e\| \lambda_{\max}(\gamma) \\
&+ \|M_M\|_{i_\infty} \|\dot{e}\| \lambda_{\max}(\gamma) \\
&+ \|e\| + \frac{1}{2}\left\|\dot{M}_M\right\|_{i_\infty} \|r\|
\end{aligned} \tag{4.35}$$

where (4.4) and its first time derivative were utilized and $C^+ \in \mathbb{R}^{3\times 11}$ denotes the pseudo–inverse of constant output matrix C which is previously defined in (3.16).

It should be noted that the following upper bound which were used in the (4.35) can be obtained from (4.5)

$$\|\dot{e}\| \leq \|r\| + \lambda_{\max}(\gamma) \|e\| . \tag{4.36}$$

Then, the inequality (4.35) can be rearranged as

$$\begin{aligned}
\left\|\widetilde{N}\right\| &\leq [\left\|M_M C\dot{A}C^+\right\|_{i_\infty} + \left\|M_M CAC^+\right\|_{i_\infty} \lambda_{\max}(\gamma) \\
&+ \left\|M_M C\dot{B}\Omega^{-1}CAC^+\right\|_{i_\infty} + \left\|M_M C\dot{B}\Omega^{-1}\right\|_{i_\infty} \lambda_{\max}(\gamma) \\
&+ \|M_M\|_{i_\infty} \lambda_{\max}^2(\gamma) + 1] \|e\| \\
&+ [\left\|M_M CAC^+\right\|_{i_\infty} + \left\|M_M C\dot{B}\Omega^{-1}\right\|_{i_\infty} \\
&+ \|M_M\|_{i_\infty} \lambda_{\max}\gamma + \frac{1}{2}\left\|\dot{M}_M\right\|_{i_\infty}] \|r\| .
\end{aligned} \tag{4.37}$$

Since all bracketed terms in (4.37) can be upper bounded with positive constants, the above inequality can be rewritten as

$$\begin{aligned}
\left\|\widetilde{N}\right\| &\leq a_1 \|e\| + a_2 \|r\| \\
&\leq \max(a_1, a_2) \|z\| \\
&\leq \rho_N \|z\|
\end{aligned} \tag{4.38}$$

where (4.10) was utilized and a_1, $a_2 \in \mathbb{R}$ are positive constants.

At this point, we are now ready to continue with the stability analysis of the proposed robust controller.

4.3. Stability Analysis

Theorem 4.3.1 *The control law in* (4.22) *and* (4.23) *ensures the boundedness of all the closed–loop signals and guarantees global exponential stability of the tracking error* $e(t)$ *in the sense that*

$$\|e(t)\| \leq \|z(0)\| \exp\left(-\frac{\overline{\epsilon}}{2}t\right) \tag{4.39}$$

provided that the p*–th diagonal entry of* β *is selected to satisfy the following condition*

$$\beta_p \geq \left|\overline{N}_p\right| \tag{4.40}$$

and its $(p-1)$*–th to* 1*–st diagonal entries are selected to satisfy the following condition*

$$\beta_i \geq \left|\overline{N}_i\right| + |\Theta_i| \tag{4.41}$$

and $k_{d,i}$*,* $\forall i = 1, \cdots, (p-1)$ *and* k_q *are selected sufficiently high with respect to the system nonlinearities.*

Proof The non–negative function, denoted by $V_1(z) \in \mathbb{R}$, is defined as

$$V_1 \triangleq \frac{1}{2}e^T e + \frac{1}{2}r^T M_M r \tag{4.42}$$

which can be lower and upper bounded as

$$\frac{1}{2}\min\{1, \underline{m}\}\|z\|^2 \leq V_1(z) \leq \frac{1}{2}\max\{1, \overline{m}\}\|z\|^2 \tag{4.43}$$

where (4.17) was utilized. The time derivative of (4.42) is obtained as

$$\begin{aligned} \dot{V}_1 &= e^T(r - \gamma e) + r^T\left(-\frac{1}{2}\dot{M}_M r - e - Kr + \widetilde{N} + \overline{N}\right) \\ &\quad -r^T\begin{bmatrix}\Phi \\ 0\end{bmatrix} + \frac{1}{2}r^T\dot{M}_M r + r^T\begin{bmatrix}\Theta \\ 0\end{bmatrix} - r^T\beta\text{Sgn}(r) \end{aligned} \tag{4.44}$$

where (4.5), (4.21), (4.28) and (4.30) were utilized. After substituting the control gain matrix K, the expression in (4.44) can be rearranged as

$$\begin{aligned} \dot{V}_1 &= -e^T\gamma e - r^T r + \left[r^T\widetilde{N} - k_q r^T r\right] \\ &\quad + \left[\sum_{i=1}^{p-1} r_i\Phi_i + \sum_{i=1}^{p-1} r_i\Theta_i - \sum_{i=1}^{p-1} k_{d,i}r_i^2\right] \\ &\quad + \left[r^T\overline{N} - r^T\beta\text{Sgn}(r)\right]. \end{aligned} \tag{4.45}$$

After utilizing (4.31), (4.32), (4.33) and (4.34), we obtain

$$\begin{aligned}\dot{V}_1 \leq & - \gamma_{\min} \|e\|^2 - \|r\|^2 + \left[\|r\| \rho_{\widetilde{N}} \|z\| - k_q \|r\|^2\right] \\ & + \left[\sum_{i=1}^{p-1} \zeta_{\Phi_i} |r_i| \|z\| - \sum_{i=1}^{p-1} k_{d,i} r_i^2\right] \\ & + |r_p| \left\{\left|\overline{N}_p\right| - \beta_p\right\} + \sum_{i=1}^{p-1} |r_i| \left\{\left|\overline{N}_i\right| + |\Theta_i| - \beta_i\right\} \end{aligned} \tag{4.46}$$

which, after completing squares for the bracketed terms and utilizing the gain conditions in (4.40) and (4.41), can be rearranged as

$$\dot{V}_1 \leq - \left[\min\left\{\gamma_{\min}, 1\right\} - \frac{\rho_{\widetilde{N}}^2}{4k_q} - \sum_{i=1}^{p-1} \frac{\zeta_{\Phi_i}^2}{4k_{d,i}}\right] \|z\|^2 . \tag{4.47}$$

When the gains $k_{d,i}$, $\forall i = 1, \cdots, (p-1)$ and k_q are selected sufficiently high, the right–hand side of the above expression can further be upper bounded as

$$\dot{V}_1 \leq -\epsilon \|z\|^2 \tag{4.48}$$

where $\epsilon \in \mathbb{R}$ is a positive constant.

Remark Before continuing with the rest of the stability analysis, we would like to highlight the procedure for choosing the entries of the control gains matrices β and K to obtain (4.48).

Step 1: The control gain matrix β is utilized to compensate for the bounded uncertain terms $\overline{N}$ and Θ. We would like to note that the terms $\overline{N}_i$ are independent of the control gains, while, from its definition in (4.30), it is clear that Θ_i depends on the $(i+1)$–th to p–th entries of β. As a result of this dependency of Θ_i from β_{i+1} to β_p, we first choose β_p, next choose β_{p-1} based on β_p, then choose β_{p-2} based on β_{p-1} and β_p, etc., and continue in a decreasing order until β_1. Specifically; for $i = p$, β_p is selected according to

$$\beta_p \geq \left|\overline{N}_p\right|$$

and from $i = p-1$ to $i = 1$, β_i are selected according to

$$\beta_i \geq \left|\overline{N}_i\right| + |\Theta_i| .$$

Step 2: Next, the scalar control gain k_q is chosen big enough to decrease the constant $\frac{\rho_{\widetilde{N}}^2}{k_q}$. It is noted that the bounding constant $\rho_{\widetilde{N}}$ does not depend on any of the control gains.

Step 3: Finally, $k_{d,i}$, $i = 1, \cdots, (p-1)$ are chosen to decrease the constant $\sum_{i=1}^{p-1} \frac{\zeta_{\Phi_i}^2}{4k_{d,i}}$. Specifically, first, $k_{d,p-1}$ is chosen to decrease the constant $\frac{\zeta_{\Phi_{p-1}}^2}{4k_{d,p-1}}$ where $\zeta_{\Phi_{p-1}}$ is the bounding constant for the uncertain term Φ_{p-1} in (4.28) which depends on $k_p = 1 + k_q$; thus, $k_{d,p-1}$ should be adjusted based on k_q. Next, $k_{d,p-2}$ is chosen to decrease the constant $\frac{\zeta_{\Phi_{p-2}}^2}{4k_{d,p-2}}$ where $\zeta_{\Phi_{p-2}}$ depends on $k_{p-1} = 1+k_q+k_{d,p-1}$ and $k_p = 1+k_q$; thus, $k_{d,p-2}$ should be adjusted based on k_q and $k_{d,p-1}$. From $i = p-3$ to $i = 1$, the rest of $k_{d,i}$ are adjusted in a similar fashion.

From (4.42), (4.43), (4.48), it is clear that $V_1(\cdot) \in \mathcal{L}_\infty$; hence $e(t)$, $r(t) \in \mathcal{L}_\infty$. Since $r(t) \in \mathcal{L}_\infty$, from (4.5), it is clear that $\dot{e}(t) \in \mathcal{L}_\infty$. Above boundedness statements and Assumption 2 can be utilized along with (4.3) and its time derivative to prove that $y(t)$, $\dot{y}(t) \in \mathcal{L}_\infty$, and thus from (3.16) and its time derivatives, it is clear that $x(t)$, $\dot{x}(t) \in \mathcal{L}_\infty$. After utilizing the above boundedness statements and Assumption 1 along with (3.15) and its time derivative, it is clear that $u(t)$, $\dot{u}(t) \in \mathcal{L}_\infty$. The above boundedness statements can be utilized along with (4.16) to prove that $\dot{r}(t) \in \mathcal{L}_\infty$. Standard signal chasing arguments can be utilized to prove that all the remaining signals remain bounded under the closed–loop operation.

Finally, after utilizing (4.43), we obtain

$$\dot{V}_1 \leq -\overline{\epsilon} V_1 \tag{4.49}$$

where $\overline{\epsilon} \triangleq \frac{2\epsilon}{\max\{1,\overline{m}\}}$ is a positive bounding constant satisfying $0 < \overline{\epsilon} \leq 1$. Solving the above differential inequality yields

$$V_1(z,t) \leq V_1(z(0),0) \exp(-\overline{\epsilon} t). \tag{4.50}$$

We can conclude as

$$\|e(t)\| \leq \|z(0)\| \exp\left(-\frac{\overline{\epsilon}}{2} t\right) \tag{4.51}$$

where (4.3), (4.42) and (4.50) were used, thus successfully meeting the tracking control objective.

CHAPTER 5

COMPUTER–BASED SIMULATIONS

In order to verify the proposed controller, it has been tested on a three DoF, nonlinear system model that was in the form of (2.1)-(2.6) by using MATLAB Simulink. Initially, the Simulink model which is obtained by using three DoF nonlinear model of HSV and its sub–blocks will be introduced, then numerical simulation parameters and results will later be examined.

5.1. Simulink Model

The Simulink model contains four main blocks as shown in Figure 5.1. In the first block which named as Aerodynamic Forces, forces in x- and z- directions and moments are calculated via velocity, AoA and dynamic pressure.

As shown in Figure 5.2 three other sub–blocks were used for this calculation. In the first sub–block, drag, lift and moment coefficients, that were necessary to obtain stability forces and moments with dynamic pressure and velocity, were calculated. Since the vehicle mass assumed to be constant, the amount of changes for center of gravity and center of pressure were assumed to be zero. These stability forces were used with the other parameters to obtain directional forces in the third sub–block.

In the second block, which is named as HSV, flight parameters were calculated by using aerodynamic forces, moments, throttle position and Mach number. As shown in Figure 5.3, this block has two sub–blocks which calculates longitudinal equations of motion and thrust, respectively.

In the third block, which is named as Atmosphere Conditions, environmental flight conditions were calculated via velocity and altitude. As shown in Figure 5.4, this block contains ISA Atmosphere Model block only as a sub–block. In the last block, which is named as Autopilot, control parameters were obtained by using controllable flight parameters. As shown in Figure 5.5, this block contains only Control block as a sub–block which used for calculate control parameters with respect to above mentioned control design.

5.2. Numerical Simulation Results

The HSV parameters used in the simulations were selected as Wilcox et al. (2010b); Wilcox (2010)

$$m = 75000 \text{ lbs} \quad Iyy = 86723 \text{ lbs.ft}^2 \quad g = 32.174 \text{ ft/s}^2. \tag{5.1}$$

Linear temperature profiles between the forebody and aftbody were used to generate elastic mode shapes and frequencies by varying the linear gradients as

$$T_{fb}(t) = 675 + 225cos\left(\frac{\pi}{10}t\right) \tag{5.2}$$

$$T_{ab}(t) = \begin{cases} 450 + 350cos\left(\frac{\pi}{3}t\right) & \text{, if } T_{fb}(t) > T_{ab}(t) \\ T_{fb}(t) & \text{otherwise.} \end{cases} \tag{5.3}$$

The natural frequencies of the elastic modes were selected according to this temperature profile as shown in Table 5.1 Wilcox et al. (2010b); Wilcox (2010) and the damping

Table 5.1. Natural Frequencies for Temperature Profiles (Nose/Tail) in Degrees

Mode	900/500	800/400	700/300	600/200	500/100
1 (Hz)	23.0	23.5	23.9	24.3	24.7
2 (Hz)	49.9	50.9	51.8	52.6	53.5
3 (Hz)	98.9	101.0	102.7	104.4	106.2

coefficient remained constant for all modes ($\xi = 0.02$).

The proposed controller is designed to follow the outputs of a well behaved reference model. To obtain these outputs, a reference model that exhibited favorable characteristics was designed from a static linearized dynamic model of the full nonlinear dynamics Bolender and Doman (2007a). The reference model outputs are shown in Figure 5.6. The velocity reference output follows a $1000ft/s$ smooth step input, while the pitch rate performs several ± 3 deg/s maneuvers. The angle of attack stays within ± 2.5 degrees.

The control gains were determined after many trials and were obtained as follows

$$K = \text{diag}\left([0.15\ 1.128\ 0.101]\right) \tag{5.4}$$

$$\beta = \text{diag}\left([0.13\ 1\ 0.1]\right) \tag{5.5}$$

$$\gamma = 2.5. \tag{5.6}$$

The HSV has an initial velocity of Mach 7.5 at an altitude of 85000 *ft*. The velocity and velocity tracking error were shown in Figure 5.7. The angle of attack and angle of

attack tracking error were shown in Figure 5.8. The pitch rate and pitch rate tracking error were shown in Figure 5.9. In addition to them, in Figure 5.10, actual and desired outputs were shown in the same figure. The control effort, other states and the structural modes are shown in Figures 5.11, 5.12 and 5.13 respectively. From Figures 5.7, 5.8, 5.9 and 5.10, it is clear that the control objective was met.

The first one second duration of the numerical simulation was depicted to better demonstrate the exponential tracking performance. The reference model outputs are shown in Figure 5.14. The velocity and velocity tracking error were shown in Figure 5.15. The angle of attack and angle of attack's tracking error were shown in Figure 5.16. The pitch rate and pitch rate tracking error were shown in Figure 5.17. In addition to them, in Figure 5.18 actual and desired outputs are shown in the same figure. It can be easily seen from Figures 5.15, 5.16, 5.17, 5.18 error values were converges to zero exponentially fast and thus the control objective was met under this one second duration.

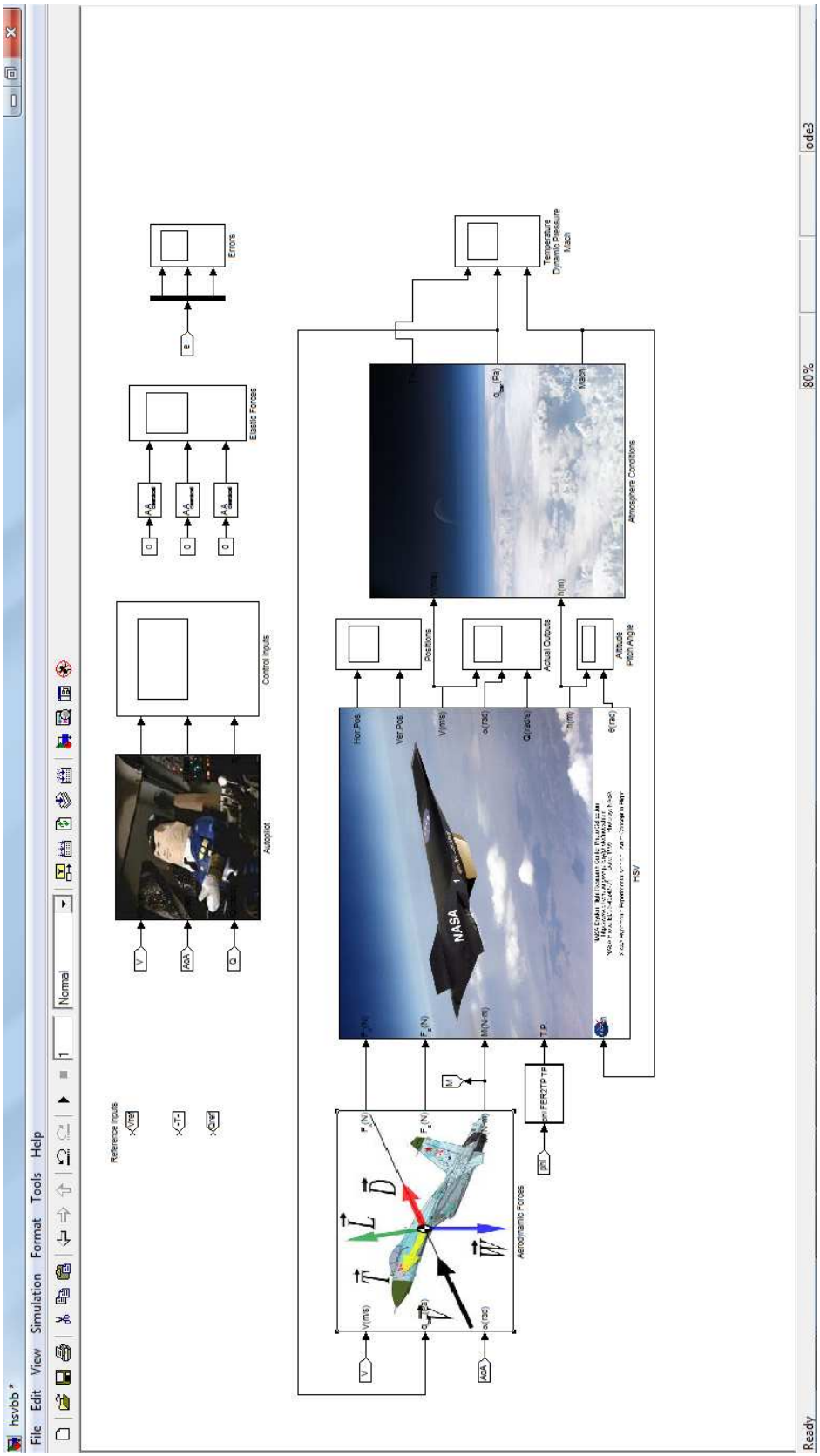

Figure 5.1. General Simulink Model.

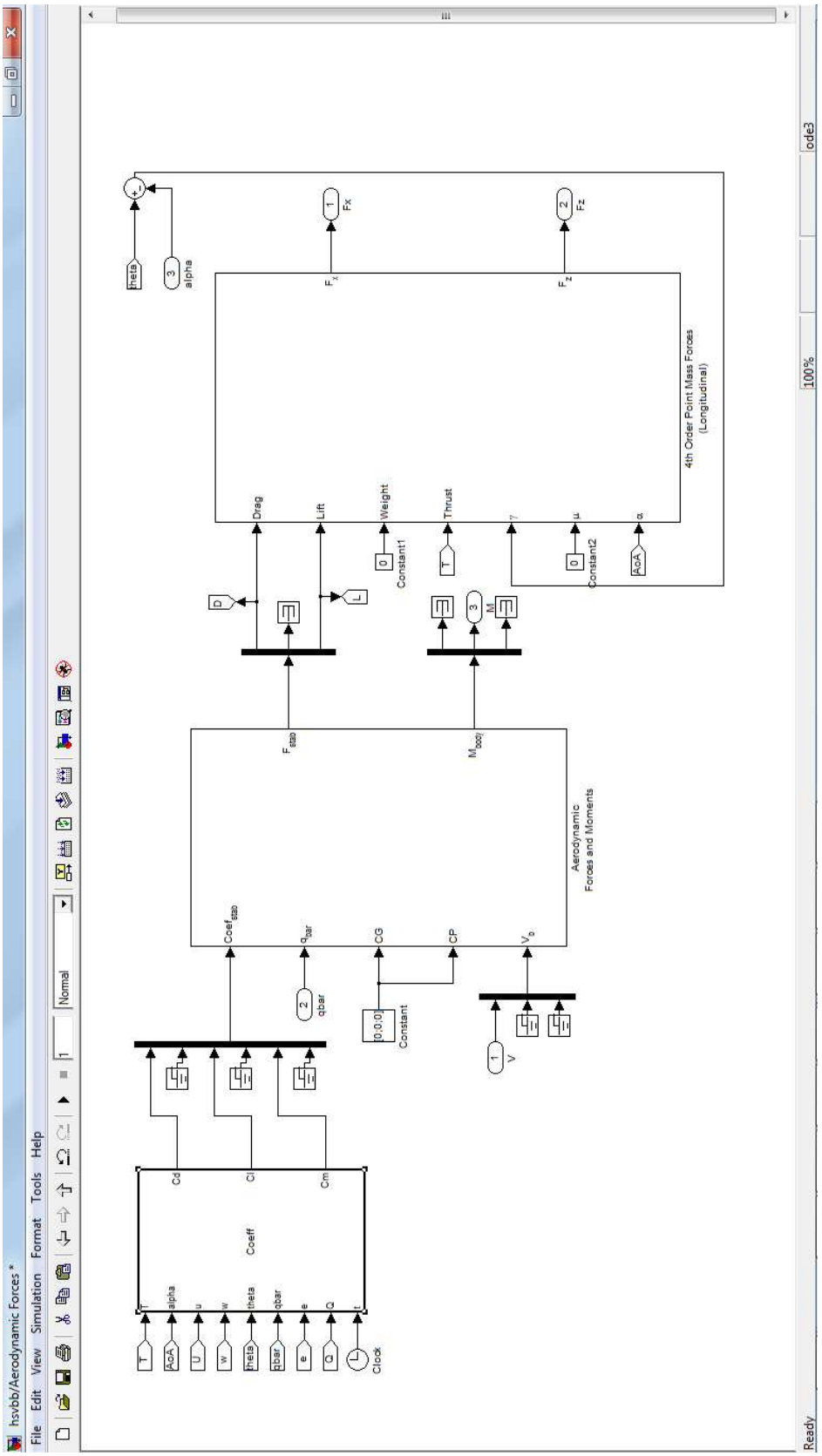

Figure 5.2. Aerodynamic Forces block.

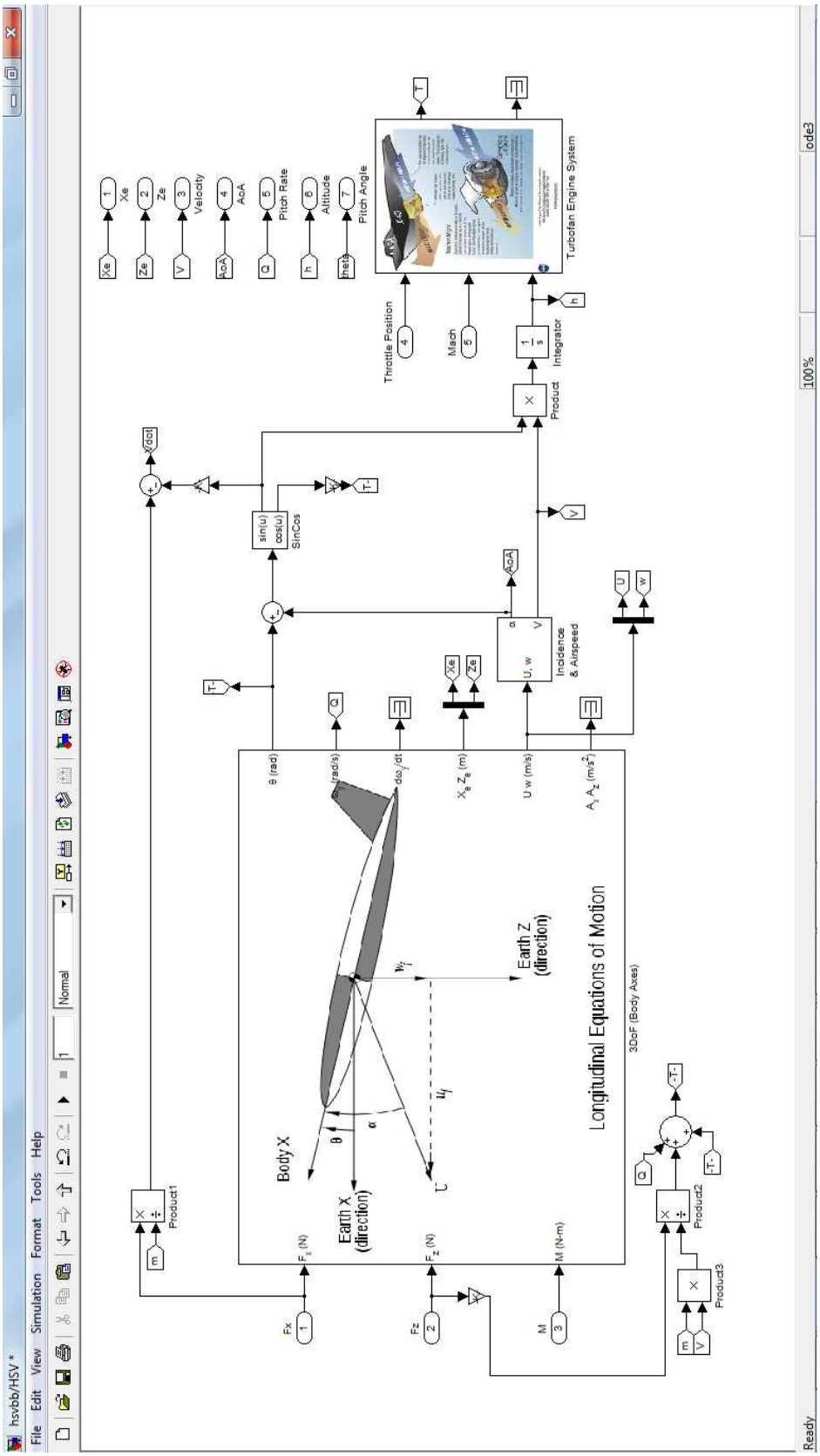

Figure 5.3. HSV block.

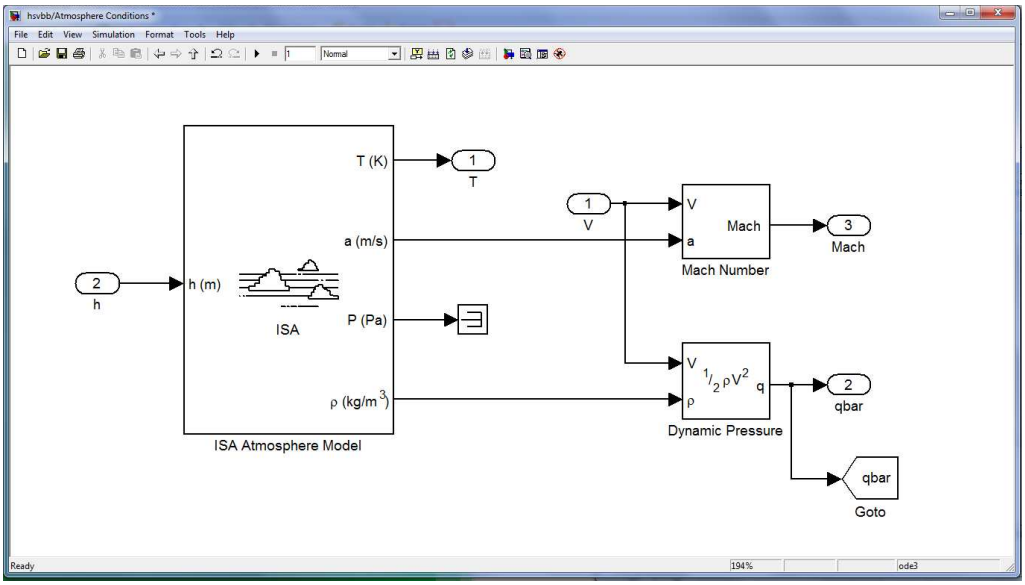

Figure 5.4. Atmosphere Conditions block.

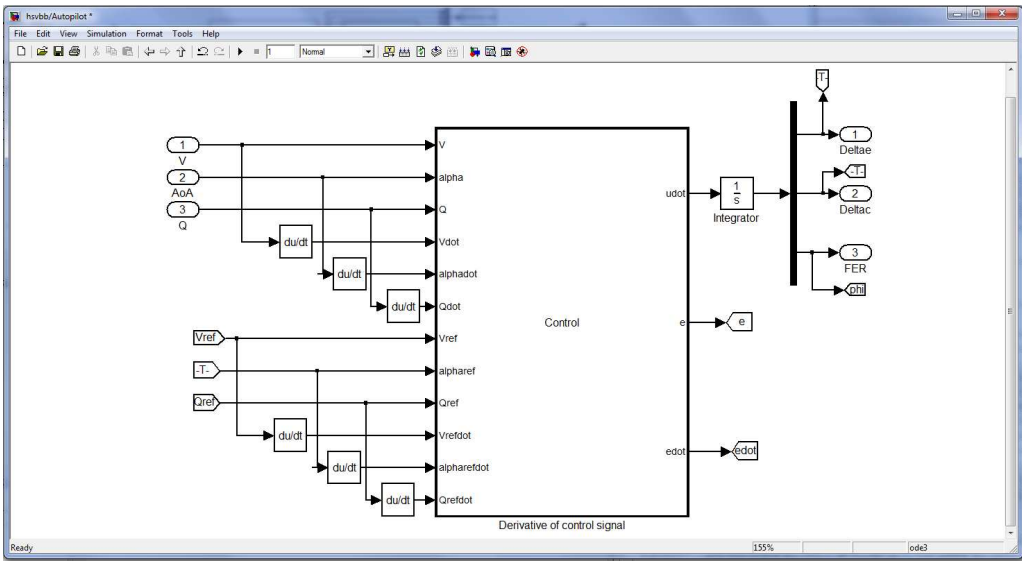

Figure 5.5. Autopilot block.

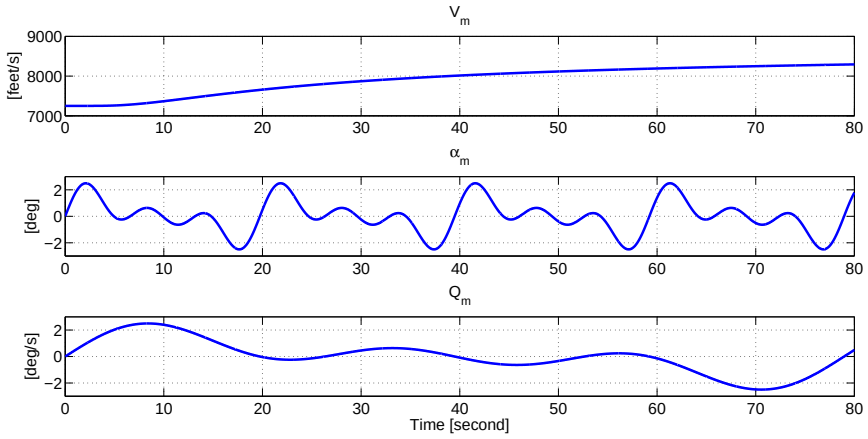

Figure 5.6. Reference model outputs $y_m(t)$. Reference Velocity $V_m(t)$, Reference AoA $\alpha_m(t)$ and Reference Pitch Rate $Q_m(t)$ are shown from top to bottom, respectively.

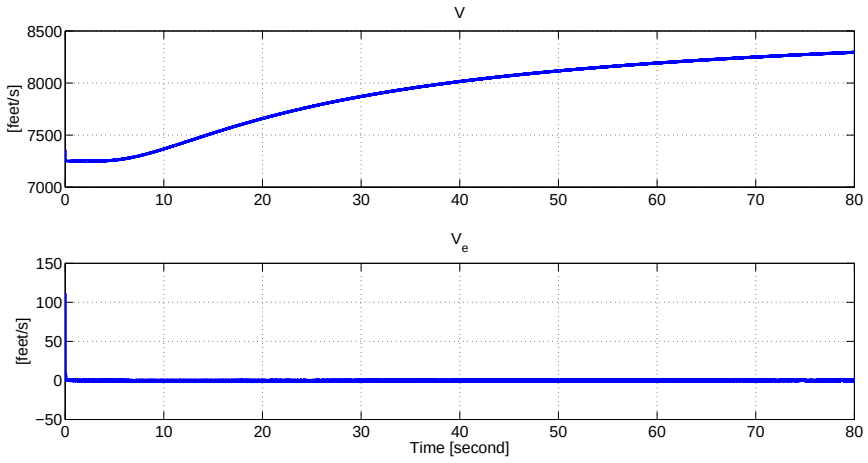

Figure 5.7. Velocity $V(t)$ at the top and Velocity Tracking Error $V_e(t)$ at the bottom.

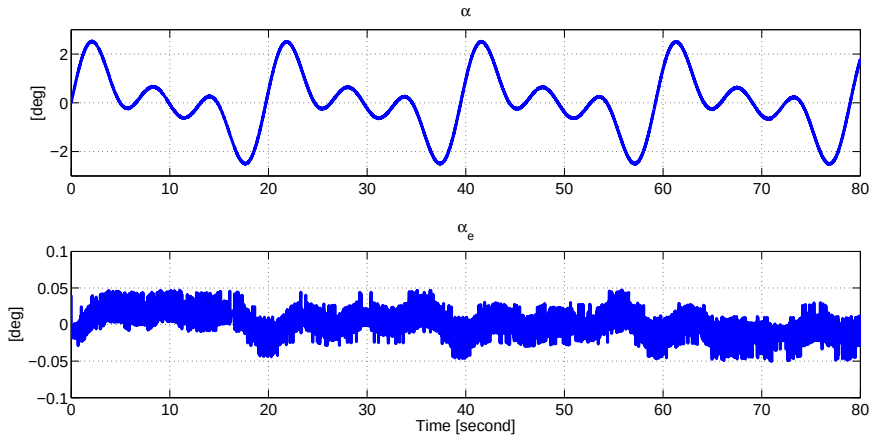

Figure 5.8. AoA $\alpha(t)$ at the top and AoA Tracking Error $\alpha_e(t)$ at the bottom.

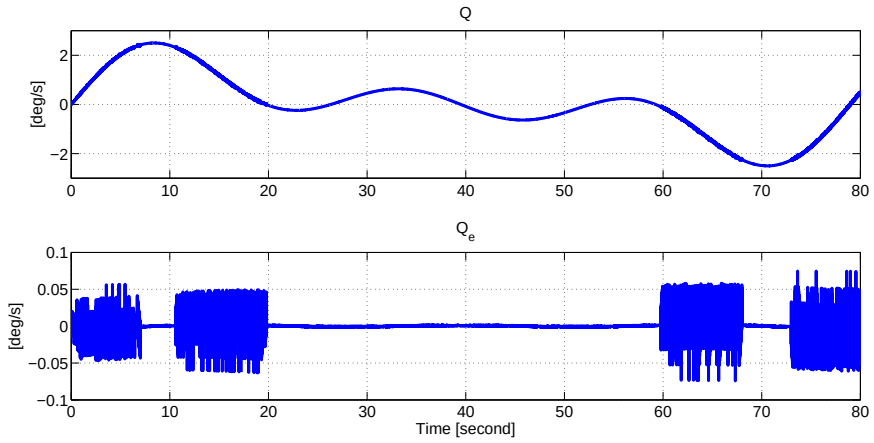

Figure 5.9. Pitch Rate $Q(t)$ at the top and Pitch Rate Tracking Error $Q_e(t)$ at the bottom.

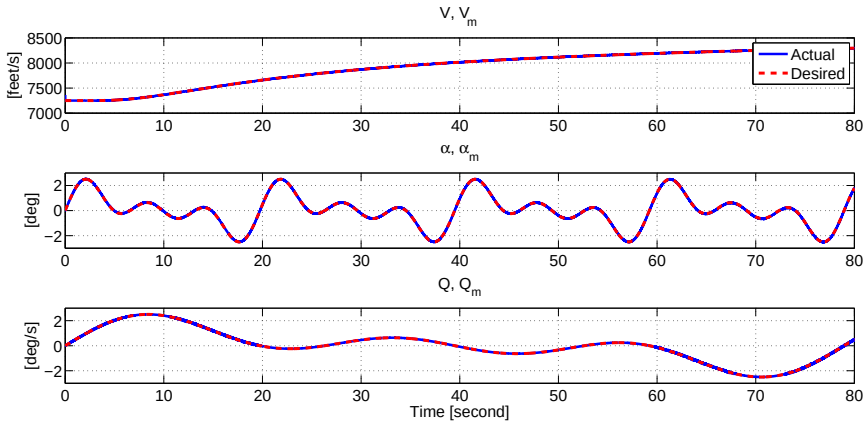

Figure 5.10. Reference Velocity $V_m(t)$ vs Actual Velocity $V(t)$, Reference AoA $\alpha_m(t)$ vs Actual AoA $\alpha(t)$ and Reference Pitch Rate $Q_m(t)$ vs Actual Pitch Rate $Q(t)$ are shown from top to bottom, respectively.

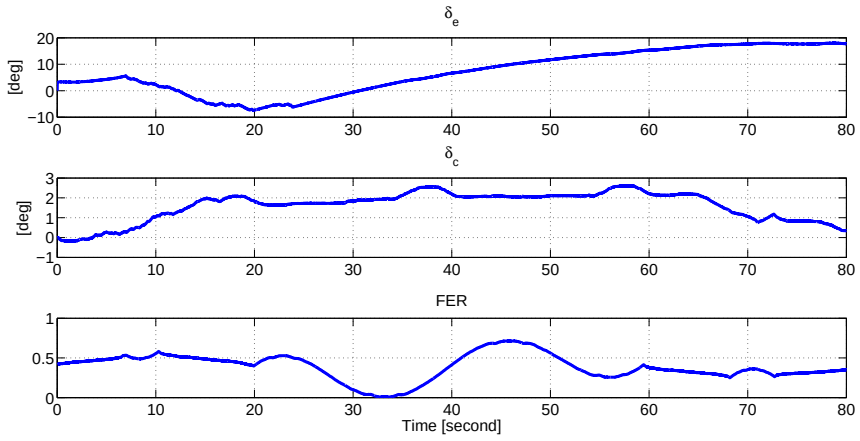

Figure 5.11. Control Inputs. Elevator deflection angle δ_e, canard deflection angle δ_c and FER are shown from top to bottom, respectively.

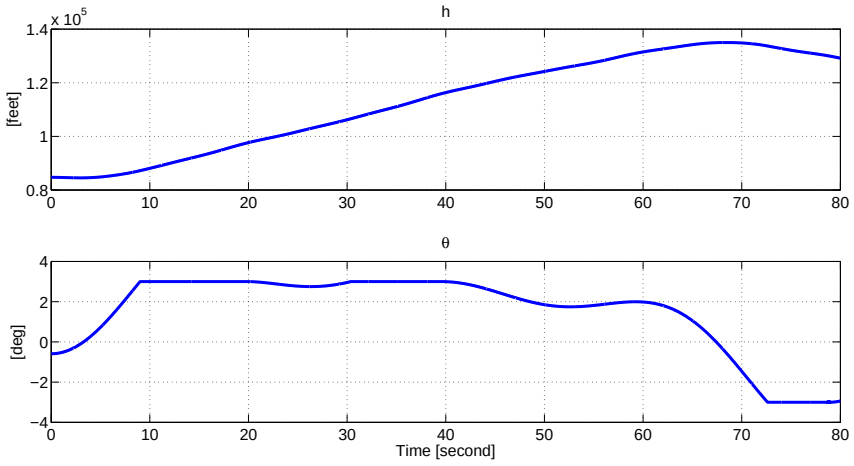

Figure 5.12. Altitude $h(t)$ at the top and Pitch Angle $\theta(t)$ at the bottom.

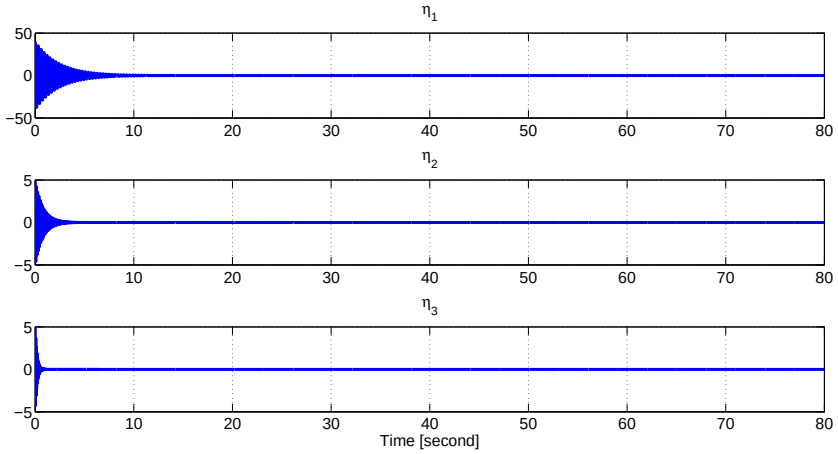

Figure 5.13. Structural Elastic Modes. First mode η_1, second mode η_2 and the third mode η_3 are shown from top to bottom, respectively.

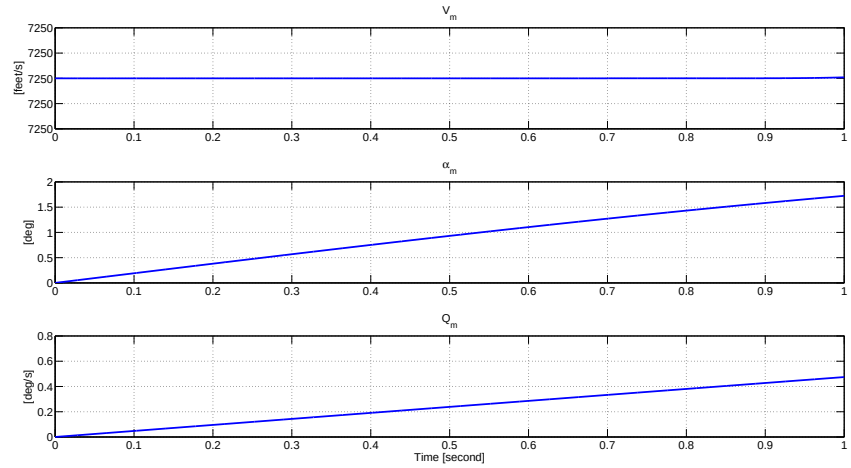

Figure 5.14. Reference model outputs $y_m(t)$. Reference Velocity $V_m(t)$, Reference AoA $\alpha_m(t)$ and Reference Pitch Rate $Q_m(t)$ are shown top to bottom, respectively.

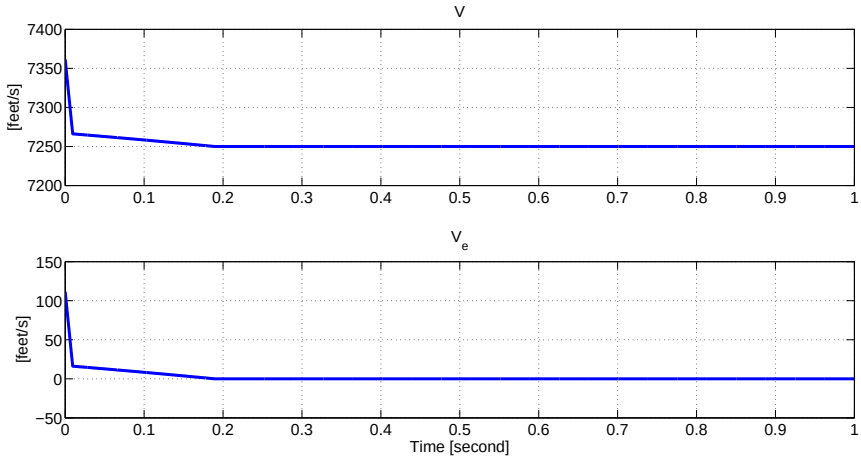

Figure 5.15. Velocity $V(t)$ at the top and Velocity Tracking Error $V_e(t)$ at the bottom.

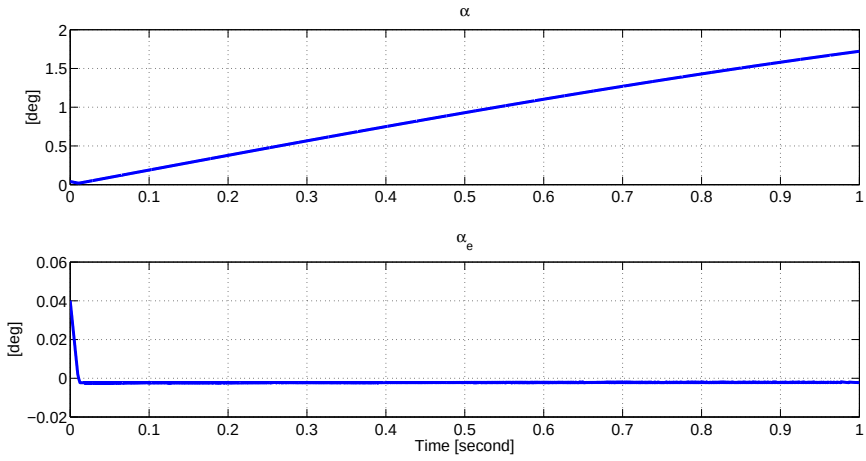

Figure 5.16. AoA $\alpha(t)$ at the top and AoA Tracking Error $\alpha_e(t)$ at the bottom.

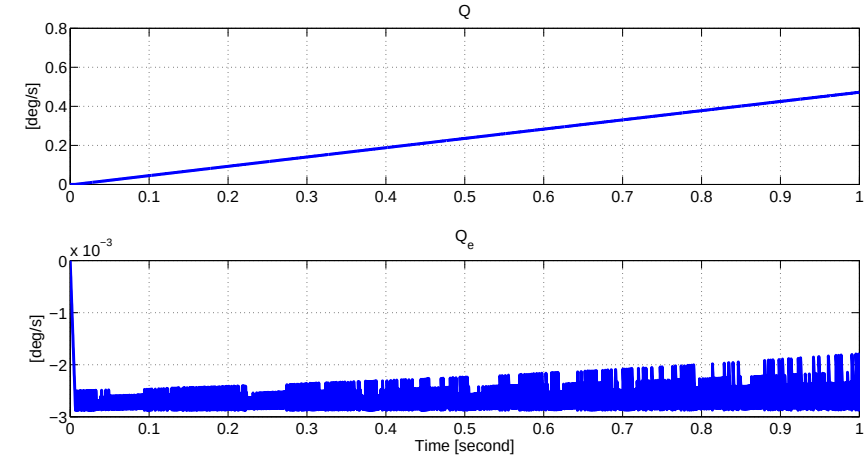

Figure 5.17. Pitch Rate $Q(t)$ at the top and Pitch Rate Tracking Error $Q_e(t)$ at the bottom.

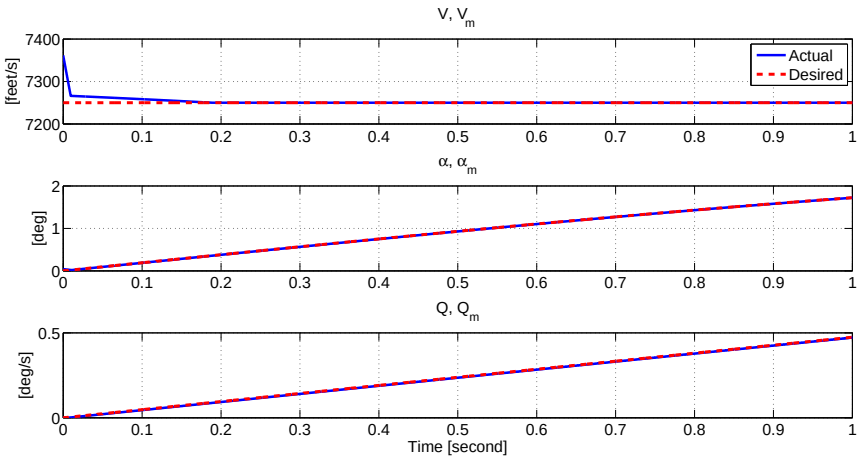

Figure 5.18. Reference Velocity $V_m(t)$ vs Actual Velocity $V(t)$, Reference AoA $\alpha_m(t)$ vs Actual AoA $\alpha(t)$ and Reference Pitch Rate $Q_m(t)$ and Actual Pitch Rate $Q(t)$ are shown from top to bottom, respectively.

CHAPTER 6

CONCLUSIONS AND FUTURE WORK

In this chapter we will mention about the conclusions and possible future works.

6.1. Conclusions

The work presented in this thesis can be divided into dynamic modelling, control design and associated stability analysis, and numerical verification.

While, initially, designing robust controllers for HSVs were aimed, the confidentiality restrictions imposed by all the sponsors of hypersonic research enforced us to start our research by deriving a dynamic model for these vehicles. To derive a dynamic model, all the basic modelling approaches utilized to model HSVs were reviewed, and a LPV dynamic model was derived. The LPV dynamic model was derived by fusing partially linearized version of the nonlinear HSV dynamics with a nonlinear state-dependent disturbance-like term. After testing our LPV model against some of the properties of the HSVs, we concluded that the model was valid.

Secondly, a novel robust control law was designed for HSVs. Specifically, the state matrix (*i.e.*, the A matrix), the input gain matrix (*i.e.*, the B matrix), and the nonlinear state-dependent disturbance-like term were considered as uncertain; and thus they were not utilized in the control design. And the output matrix (*i.e.*, the C matrix) was considered as available. In the open-loop error development, we encountered an uncertain matrix which was non-symmetric and sign indefinite. To deal with this uncertain matrix, a matrix decomposition method was employed. This decomposition yielded a three uncertain matrices one of which was assumed to be available for the control design. While this assumption seemed to be restricting our method, applying the decomposition to the publicly available HSV models resulted in that particular matrix being equal to the identity matrix. After this, the open-loop error dynamics were obtained and the robust controller was designed. The controller was obtained by fusing a PI-like controller with integral of the signum of the error terms for robustness (*i.e.*, uncertainty compensation). At this point, we would like to highlight that the when signum of the error terms are uti-

lized the control researchers think about sliding mode controllers. Our design is different than the sliding mode controllers in the sense that we utilized the 'integral' of the signum of the error terms. This integration resulted in our controller to be continuous unlike the discontinuous sliding mode controllers. After obtaining the closed-loop error system, to verify the type of the stability, we continued with the stability analysis. In the stability analysis, Lyapunov-type techniques were utilized. Particularly, a non-negative Lyapunov function was chosen and its time derivative was shown to be less than or equal to some negative constant times itself. Mathematically speaking, global exponential stability of the tracking error and its time derivative was ensured. This concluded the control design.

Finally, to numerically verify the proposed controller, a numerical simulation was conducted with Matlab/Simulink. In the numerical simulations, the proposed controller was applied to the actual nonlinear HSV dynamics. Consistent with the mathematical verification, in the numerical simulations, exact tracking of the reference trajectories were observed in less than one second. At this point, we would like to note that the derived dynamic model was only utilized to simulate the behavior of the HSV and it was not utilized in any part of the control design.

Although the controller obtained via partially linearized model, it can apply to the nonlinear dynamic model and gives satisfactory results. It shows that LPV approach with exogenous disturbances provides a good approximation to the nonlinear model.

6.2. Future Work

There is much to be considered as future work. As very well known to the nonlinear control researchers, robust control strategies are usually designed based on the worst-case scenario in the sense that when needed the 'maximum values' of the uncertainties that they can reach are considered in the design of the controllers. This results in a need for an increased amount of control effort. On the other hand, adaptive control strategies employ and update rule to compensate for structured uncertainties. In view of these, a possible focus of future research may be designing robust adaptive controllers for HSVs to reduce the required control effort. Another possible future research may be employing optimal control techniques to efficiently use the resources on the HSV.

Another possible focus of future research may be applying the proposed robust controller to other applications that are represented with an LPV model. It is our sincere belief that with only a small modification, the proposed controller can be applied to some other systems as well. However, since, in several aircrafts, acceleration measure-

ments are available, our control design utilized these measurements. On the other hand, in some mechatronic systems, to reduce the cost, acceleration are not measured. To address this issue, future research could focus on removing acceleration or maybe even velocity measurement (*i.e.*, output feedback).

REFERENCES

Abbasa, L. K., C. Qian, P. Marzocca, G. Zafer, and A. Mostafa (2008). Active aerothermoelastic control of hypersonic double-wedge lifting surface. *Chin. Journal Aeronaut 21*(4), 8–18.

Adami, T., J. Zhu, M. Bolender, D. Doman, and M. Oppenheimer (2006). Flight control of hypersonic scramjet vehicles using a differential algebraic approach. In *AIAA Guidance, Navigation and Control Conference*, Keystone, CO, USA.

Anderson, J. (2002). *Modern Compressible Flow, 3rd Edition*. USA: McGraw-Hill.

Anderson, J. (2006). *Hypersonic and High-Temperature Gas Dynamics*. USA: AIAA Education Series.

Austin, K. J. and P. A. Jacobs (2001). Application of genetic algorithms to hypersonic flight control. In *IFSA World Congr., NAFIPS Int. Conf.*, Vancouver, British Columbia, Canada, pp. 2428–2433.

Baldelli, D., R. Lind, and M. Brenner (2005). Nonlinear aeroelastic aeroservoelastic modelling by block-oriented identification. *Journal of Guidance, Control and Dynamics 28*(5), 2056–2064.

Baumann, E., C. Bahm, B. Strovers, R. Beck, and M. Richard (2008). Yhe x-43a six dof monte carlo analysis. In *46th Aerospace Sciences Meeting and Exhibit*, St. Louis, MO, USA, pp. 2203–2210.

Berry, S., A. Auslender, A. Diller, and J. F. Calleja (2001). Hypersonic boundary-layer trip development for hyper-x. *Journal of Spacecraft and Rockets 38*(6), 853–864.

Berry, S., K. Daryabeigi, K. Wurster, and R. Bittner (2008). Boundary layer transition on x-43a. In *38th Fluid Dynamics Conference and Exhibit*, Seattle, WA, USA.

Bertin, J. J. (1994). *Hypersonic Aerothermodynamics*. USA: AIAA Education Series.

Bertin, J. J., J. Periaux, and J. Ballmann (1992). *Advances in Hypersonics: Defining the Hypersonic Environment, Volume 1*. Boston, MA, USA: Birkhauser.

Bhat, S. (2008). Control-oriented analysis of aerothermoelastic effects for a hypersonic vehicle.

Bolender, M. and D. Doman (2005). A nonlinear model for the longitudinal dynamics of a hypersonic air-breathing vehicle. In *AIAA Guidance, Navigation and Control Conference and Exhibit*, San Francisco, CA, USA, pp. 1–22.

Bolender, M. and D. Doman (2006). Modelling unsteady heating effects on the structural dynamics of a hypersonic vehicle. In *AIAA Atmospheric Flight Mechanics Conference and Exhibit*, Colorado, USA.

Bolender, M. and D. Doman (2007a). A nonlinear longitudinal dynamical model of an air-breathing hypersonic vehicle. *Journal of Spacecraft and Rockets 44*(2), 374–387.

Bolender, M. and D. Doman (2007b). Nonlinear longitudinal dynamical model of an air-breathing hypersonic vehicle. *Journal of Spacecraft and Rockets 44*(2), 374–387.

Bolender, M., M. Oppenheimer, and D. Doman (2007). Effects of unsteady and viscous aerodynamics on the dynamics of a flexible air-breathing hypersonic vehicle. *AIAA paper*.

Buschek, H. and A. Calise (1993). Robust control of hypersonic vehicles considering propulsive and aeroelastic effects. In *AIAA Guidance, Navigation and Control Conference*, Monterrey, CA, USA, pp. 550–560.

Buschek, H. and A. Calise (1994). Fixed order robust control design for hypersonic vehicles. In *AIAA Guidance, Navigation and Control Conference*, Scottsdale, AZ, USA, pp. 1094–1103.

Chavez, F. and D. Schmidt (1994). Analytical aeropropulsive/aeroelastic hypersonic vehicle model with dynamic analysis. *Journal of Guidance, Control and Dynamics 17*(6), 1308–1319.

Chen, J., A. Behal, and D. M. Dawson (2008). Robust feedback control for a class of

uncertain MIMO nonlinear systems. *IEEE Transactions and Automatic Control 53*(2), 591–596.

Cockrell, J. C. E., A. H. Auslender, R. W. Guy, C. R. McClinton, and S. S. Welch (2002). Technology roadmap for dual-mode scramjet propulsion to support space-access vision vehicle development. In *AIAA/AAAF International Space Planes and Hypersonic Systems and Technologies Conference*, Orleans, France, pp. 1–14.

Costa, R. R., L. Hsu, A. K. Imai, and P. Kokotovic (2003). Lyapunov-based adaptive control of MIMO systems. *Automatica 39*(7), 1251–1257.

Culler, A., T. Williams, and M. Bolender (2007). Aerothermal modelling and dynamic analysis of a hypersonic vehicle. In *AIAA Atmospheric Flight Mechanics Conference and Exhibit*, SC, USA.

Dickeson, J., A. Rodriguez, S. Sridharan, J. Benavides, D. Soloway, A. Kelkar, and J. Vogel (2009). Decentralized control of an airbreathing scramjet-powered hypersonic vehicle. In *AIAA Conference on Guidance, Navigation and Control*, Chigago, IL, USA, pp. 1–25.

Dolvin, D. (2008). Hypersonic international flight research and experimentation (hifire) fundamental science and technology development strategy. In *15th AIAA International Space Planes and Hypersonic Systems and Technologies Conference*, Dayton, OH, USA, pp. 2586–2592.

Doman, D., M. Oppenheimer, and M. Bolender (2006). Progress in guidance and control research for space access and hypersonic vehicles. Technical report, Air Force Research Laboratory, Wright Patterson Air Force Base.

Fidan, B., M. Mirmirani, and P. Ioannou (2003). Flight dynamics and control of air-breathing hypersonic vehicles: Review and new directions. In *12th AIAA/AHI Space Planes and Hypersonic Systems and Technologies Conference*, Norfolk, VA, USA, pp. 7081–7087.

Fiorentini, L. (2010). *Nonlinear Adaptive Controller Design For Air-Breathing Hypersonic Vehicles*. Ph. D. thesis, Ohio State University, Ohio, USA.

Fiorentini, L., A. Serrani, M. Bolender, and D. Doman (2007). Nonlinear robust/adaptive controller design for an air-breathing hypersonic vehicle model. In *AIAA Guidance, Navigation and Control Conference and Exhibit*, SC, USA.

Gibson, T., L. Crespo, and A. Annaswamy (2009). Adaptive control of hypersonic vehicles in the presence of modeling uncertainties. In *American Control Conference*, St. Louis, MO, USA.

Gilbert, M. G., J. Heeg, A. S. Potozky, C. V. Spain, D. L. Scistmann, and H. J. Dunn (1990, January). The application of active controls technology to a generic aircraft configuration. Technical Report NAS 1.15101689, NASA.

Glass, D. (2008). Ceramic matrix composite (cmc) thermal protection systems (tps) and hot structures for hypersonic vehicles. In *AIAA International Space Planes and Hypersonic Systems and Technologies Conference*, Dayton, OH, USA, pp. 1–36.

Groves, P., A. Serrani, S. Yurkovich, M. Bolender, and D. Doman (2006). Anti-windup control for an air-breathing hypersonic vehicle model. *AIAA paper*.

Groves, P., D. Sigthorsson, A. Serrani, S. Yurkovich, M. Bolender, and D. Doman (2005). Reference command tracking for a linearized model of an air-breathing hypersonic vehicle. *AIAA paper*.

Hank, J., J. Murphy, and R. Mutzman (2008). Hypersonic international flight research and experimentation (hifire) fundamental science and technology development strategy. In *The X-51A Scramjet Engine Flight Demonstration Program*, Dayton, OH, USA, pp. 2540–2546.

Heeg, J., M. G. Gilbert, and A. S. Pototzky (1993). Active control of aerothermoelastic effects for a conceptual hypersonic aircraft. *Journal of Aircraft 30*(4), 453–458.

Heeg, J., T. A. Zieler, A. S. Potozky, C. V. Spain, and W. C.Englend (1993, October). X-43a hypersonic vehicle technology development. Technical Report NAS 1.15109007, Aerothermoelastic Analysis of a NASP Demonstrator Model.

Heiser, W. H., D. Pratt, D. Daley, and U. Mehta (1994a). A hypersonic vehicle model using developed with piston theory. *AIAA paper*.

Heiser, W. H., D. T. Pratt, D. Daley, and U. Mehta (1994b). *Hypersonic Airbreathing Propulsion*. USA: AIAA Education Series.

Huo, Y., M. Mirmirani, P. Ioannou, and M. Kuipers (2006). Altitude and velocity tracking control for an air-breathing hypersonic cruise vehicle. *AIAA paper*.

Korad, A. S. (2010, May). Modeling, analysis, and control of a hypersonic vehicle with significant aero-thermo-elastic-propulsion interactions, and propulsive uncertainty.

Kuipers, M., M. Mirmirani, P. Ioannou, and Y. Huo (2007a). Adaptive control of an aeroelastic air-breathing hypersonic cruise vehicle. *AIAA paper*.

Kuipers, M., M. Mirmirani, P. Ioannou, and Y. Huo (2007b). Adaptive control of an aeroelastic air-breathing hypersonic cruise vehicle. *AIAA paper*.

Kumar, A., J. P. Drummond, C. R. McClinton, and J. L. Hunt (2001, September). Research in hypersonic airbreathing propulsion at the NASA langley research center. Technical Report ISABE-2001-4, NASA.

Lind, R. (2001). Linear parameter-varying modelling and control of structural dynamics with aeroelastic effects. *Journal of Guidance, Control and Dynamics 25*(4), 733–739.

Lind, R. and M. Brenner (1999). *Robust Aeroservoelastic Atability Analysis: Flight Test Applications*. USA: Springer.

Marrison, C. I. and R. F. Stengel (1998). Design of robust control systems for a hypersonic aircraft. *Journal of Guidance, Control and Dynamics 21*(1), 58–63.

Marshall, L., G. Corpening, and R. Sherrill (2005). A chief engineerâs view of the NASA x-43a scramjet flight test. In *AIAA/CIRA 13th International Space Planes and Hypersonics Systems and Tech. Conference*.

McClinton, C. R. (2007). X-43 scramjet power breaks the hypersonic barrier dryden lectureship in research for 2006. In *44th AIAA Aerospace Sciences Meeting and Exhibit*, Reno, Nevada, USA, pp. 1–18.

Mirmirani, M., C. Wu, A. Clark, S. Choi, and R. Colgren (2005). Modelling for control

of a generic air-breathing hypersonic vehicle. *AIAA paper*.

Morse, A. S. (1993). A gain matrix decomposition and some of its applications. *Systems & Control Letters 21*(1), 1–10.

Oppenheimer, M. and D. Doman (2006a). A hypersonic vehicle model developed with piston theory. Technical report, Air Force Research Laboratory (AFRL), Wright Patterson Air Force Base.

Oppenheimer, M. and D. Doman (2006b). A hypersonic vehicle model using developed with piston theory. *AIAA paper*.

Oppenheimer, M., D. Doman, M. Bolender, and T. Skujins (2007). A flexible hypersonic vehicle model developed with piston theory. *AIAA paper*.

Parker, J., A. Serrani, S. Yurkovich, M. Bolender, and D. Doman (2005). Approximate feedback linerization of an air-breathing hypersonic vehicle. Technical report, Air Force Research Laboratory (AFRL), Wright Patterson Air Force Base.

Parker, J., A. Serrani, S. Yurkovich, M. Bolender, and D. Doman (2007). Control oriented modelling of an air-breathing hypersonic vehicle. *AIAA Journal of Guidance, Control, and Dynamics*.

Peebles, C. (2008). *Road to Mach 10: Lessons Learned from the X-43A Flight Research Program*. Reston, VA, USA: AIAA Education Series.

Potozky, A. S., C. V. Spain, D. L. Spain, and T. E. Noll (1988, September). Application of unsteady aeroelastic analysis techniques on the national aerospace plane. Technical Report NAS 1.15100648, NASA.

Rausch, V. L., C. R. McClinton, and J. L. Crawford (1997). Hyper-x flight validation of hypersonic airbreathing technology. Technical Report ISABE-97-7024, NASA.

R.McClinton, C. (2007). X-43 scramjet power breaks the hypersonic barrier dryden lectureship in research for 2006. In *44th AIAA Aerospace Sciences Meeting and Exhibit*, Reno, NV, USA, pp. 1–18.

Rodriguez, A. A. (2004). *Analysis and Design of Multivariable Feedback Control Systems*. USA: Control3D Education Series.

Rodriguez, A. A., J. J. Dickeson, S. Sridharan, A. Khorad, J. Khatri, J. Benavides, D. Soloway, A. Kelkar, and J. M. Vogel (2009). Control-relevant modeling, analysis, and design for scramjet-powered hypersonic vehicles. In *AIAA/DLR/DGLR International Space Planes and Hypersonic Systems and Technologies Conference*, St. Louis, Missouri, USA, pp. 3154–3159.

Serrani, A., A. Zinnecker, L. Fiorentini, M. Bolender, and D. Doman (2009). Integrated adaptive guidance and control of constrained nonlinear air-breathing hypersonic vehicle models. In *American Control Conference*, St. Louis, MO, USA.

Sigthorsson, D., A. Serrani, S. Yurkovich, M. Bolender, and D. Doman (2006). Tracking control for an overactuated hypersonic air-breathing vehicle with steady state constraints. *AIAA paper*.

Sigthorsson, O. D., P. Jankovsky, A. Serrani, S. Yurkovich, M. Bolender, and D. Doman (2008). Robust linear output feedback control of an air-breathing hypersonic vehicle. *Journal of Guidance, Control and Dynamics 31*(4), 1052–1066.

Smart, M., N. Hass, and A. Paull (2006). Flight data analysis of the hyshot 2 scramjet flight experiment. *AIAA Journal 44*(10), 2366–2375.

Soloway, D., A. Rodriguez, J. Dickeson, O. Cifdaloz, J. Benavides, S. Sridharan, A. Kelkar, and J. Vogel (2009). Constraint enforcement for scramjet-powered hypersonic vehicles with significant aero-elastic-propulsion interactions. In *American Control Conference*, St. Louis, MO, USA, pp. 3154–3159.

Starkey, R., D. Liu, R. Chang, and P. Chem (2008). Rapid conceptual design and analysis of a hypersonic air-breathing missile. In *AIAA International Space Planes and Hypersonic Systems and Technologies Conference*, Dayton, OH, USA.

Stien, G. (2003). Respect the unstable. *IEEE Control Systems Magazine*, 12–25.

Tao, G. (2003). *Adaptive Control Design and Analysis*. New York, NY, USA: John Wiley and Sons.

Voland, R. T., L. D. Huebner, and C. R. McClinton (2005). X-43a hypersonic vehicle technology development. Technical Report IAC-05-D2.6.01, NASA Langley Research Center, Hampton, VA.

Walker, S., F. Rodgers, A. Paull, and D. V. Wie (2008). Hycause flight test program. In *15th AIAA International Space Planes and Hypersonic Systems and Technologies Conference*, Dayton, OH, USA, pp. 2580–2586.

Wang, Q. and R. F. Stengel (2000). Robust nonlinear control of a hypersonic aircraft. *Journal of Guidance, Control and Dynamics 23*(4), 577–585.

Wilcox, Z. D. (2010). *Nonlinear Control of Linear Parameter Varying Systems with Applications to Hypersonic Vehicles*. Ph. D. thesis, University of Florida, Florida, USA.

Wilcox, Z. D., W. MacKunis, Bhat, R. Lind, and W. E. Dixon (2010a). Lyapunov-based exponential tracing control of a hypersonic aircraft with aerothermoelastic effects. *Journal of Guidance, Control and Dynamics 33*(4), 1213–1224.

Wilcox, Z. D., W. MacKunis, S. Bhat, R. Lind, and W. E. Dixon (2010b). Lyapunov-based exponential tracking control of a hypersonic aircraft with aerothermoelastic effects. *Journal of Guidance, Control and Dynamics 33*(4), 1213–1224.

Williams, T., M. Bolender, D. Doman, and O. Morataya (2006a). An aerothermal flexible model analysis of a hypersonic vehicle. In *AIAA Atmospheric Flight Mechanics Conference and Exhibit*, Colorado, USA.

Williams, T., M. A. Bolender, D. B. Doman, and O. Morataya (2006b). An aerothermal flexible mode analysis of a hypersonic vehicle. *AIAA Paper*.

Yoshihiko, M. (2003). Adaptive gain-scheduled h-infinity control of linear parameter varying systems with nonlinear components. In *American Control Conference*, Denver, CO, USA, pp. 208–213.